Journal of Quantitative Spectroscopy & Radiative Transfer 113 (2012) 1013–1033

Contents lists available at SciVerse ScienceDirect

Journal of Quantitative Spectroscopy & Radiative Transfer

journal homepage: www.elsevier.com/locate/jqsrt

Spectral line parameters including temperature dependences of self- and air-broadening in the 2←0 band of CO at 2.3 μm

V. Malathy Devi [a,*], D. Chris Benner [a], M.A.H. Smith [b], A.W. Mantz [c], K. Sung [d], L.R. Brown [d], A. Predoi-Cross [e]

[a] Dept. of Physics, The College of William and Mary, Box 8795, Williamsburg, VA 23187, USA
[b] Science Directorate, NASA Langley Research Center, Hampton, VA 23681, USA
[c] Dept. of Physics, Astronomy and Geophysics, Connecticut College, 270 Mohegan Avenue, New London, CT 06320, USA
[d] Jet Propulsion Laboratory, California Institute of Technology, 4800 Oak Grove Dr., Pasadena, CA 91109, USA
[e] Dept. of Physics and Astronomy, The University of Lethbridge, 4401 University Drive, Lethbridge, Alta., Canada TIK 3M4

ARTICLE INFO

Available online 19 February 2012

Keywords:
CO
Lorentz widths
Pressure shifts
Line mixing
Temperature dependences of Lorentz widths and shifts
Off-diagonal relaxation matrix elements
Temperature dependence of line mixing

ABSTRACT

Temperature dependences of pressure-broadened half-width and pressure-induced shift coefficients along with accurate positions and intensities have been determined for transitions in the 2←0 band of $^{12}C^{16}O$ from analyzing high-resolution and high signal-to-noise spectra recorded with two different Fourier transform spectrometers. A total of 28 spectra, 16 self-broadened and 12 air-broadened, recorded using high-purity ($\geq$99.5% ^{12}C-enriched) CO samples and CO diluted with dry air (research grade) at different temperatures and pressures, were analyzed simultaneously to maximize the accuracy of the retrieved parameters. The sample temperatures ranged from 150 to 298 K and the total pressures varied between 5 and 700 Torr. A multispectrum nonlinear least squares spectrum fitting technique was used to adjust the rovibrational constants (G, B, D, etc.) and intensity parameters (including Herman–Wallis coefficients), rather than determining individual line positions and intensities. Self- and air-broadened Lorentz half-width coefficients, their temperature dependence exponents, self- and air-pressure-induced shift coefficients, their temperature dependences, self- and air- line mixing coefficients, their temperature dependences and speed dependence have been retrieved from the analysis. Speed-dependent line shapes with line mixing employing off-diagonal relaxation matrix element formalism were needed to minimize the fit residuals. This study presents a precise and complete set of spectral line parameters that consistently reproduce the spectrum of carbon monoxide over terrestrial atmospheric conditions.

© 2012 Elsevier Ltd. All rights reserved.

1. Introduction

CO is one of the most studied diatomic molecules spanning more than a century. Its infrared spectra have been the subject of perhaps hundreds of investigations. A large number of high-resolution measurements of spectral line shape parameters of CO have been cited in the literature. They extend from the basic measurements involving line positions and intensities to sophisticated measurements of line shape parameters such as collisional broadening, Dicke narrowing, pressure-induced shifts, temperature dependences of pressure-broadening and collisional line mixing.

The present measurements were undertaken because several instrument concepts under study for upcoming

* Corresponding author. Tel.: +1 757 864 5521; fax: +1 757 864 7790.
E-mail addresses: malathy.d.venkataraman@nasa.gov, malathyv@hotmail.com (V. Malathy Devi).

0022-4073/$ - see front matter © 2012 Elsevier Ltd. All rights reserved.
doi:10.1016/j.jqsrt.2012.02.010

Earth Science Decadal Survey satellite missions (most notably Active Sensing of CO_2 Emissions over Nights, Days and Seasons [ASCENDS], Geostationary Coastal and Air Pollution Events [GEO-CAPE] and Global Atmospheric Composition Mission [GACM]), plan to use observed radiances in the 2.3-μm spectral region to retrieve atmospheric profiles of CO. Accurate knowledge of air-broadening parameters is needed for tropospheric retrievals, but self-broadened widths and shifts and their temperature dependences are required for atmospheric sensors that utilize gas correlation cells [e.g., Measurements of Air Pollution from Satellites (MAPS), Measurements Of Pollution In The Troposphere (MOPITT), ASCENDS]. While the spectroscopic databases such as HITRAN04 [1] and HITRAN08 [2] already contain significant information on CO, the line parameters in the 2.3-μm spectral region do not have sufficient accuracy (1%) required for ASCENDS retrievals. The present study provides high-resolution laboratory spectroscopy of the CO $2\leftarrow0$ band at 2.3-μm over the range of terrestrial atmospheric temperatures and pressures. Laboratory spectra recorded with two different high-resolution Fourier transform spectrometers and temperature-controlled sample cells are analyzed using a thoroughly tested multispectrum nonlinear least squares fitting technique to retrieve the required parameters. A consistent and accurate set of retrievals is reported for line positions, intensities, self- and air-broadened widths, and self- and air- pressure-induced line shifts, along with their temperature dependences. Most importantly, line mixing (also known as line coupling) and other non-Voigt effects such as speed dependence are quantitatively assessed.

The CO $2\leftarrow0$ band is significant for atmospheric remote sensing because combined observations in the $1\leftarrow0$ and $2\leftarrow0$ bands allow the improved determination of the amount of tropospheric CO from nadir-viewing observations. Independent measurements of air-broadening and pressure-induced shift parameters and their temperature dependences are desirable. Current values in HITRAN08 [2] for the CO $2\leftarrow0$ band are based upon only one published laboratory study by Zou and Varanasi [3] who reported self- and air-broadening in both the $1\leftarrow0$ and $2\leftarrow0$ bands of $^{12}C^{16}O$ by analyzing spectra recorded at several temperatures between 174 and 296 K with a Bruker IFS-120HR Fourier transform spectrometer. For the $2\leftarrow0$ band, they reported direct air-broadening coefficients and their temperature dependences for transitions with $|m|\leq18$. Their analysis involved a conventional Voigt line shape with no line mixing or speed dependence. They applied a multispectrum fitting technique just to narrow spectral intervals, and retrieved simultaneously a few spectra (8) recorded at each set of temperatures, rather than using all the data at the same time. The uncertainties reported in their retrieved parameters are much larger than those in the present study.

No studies of air-broadened line mixing in the CO $2\leftarrow0$ band were reported previously, but self-line mixing in the $2\leftarrow0$ band was studied by Brault et al. [4] using CO sample pressures $P\leq600$ Torr. Their best-fit model included speed-dependent line shape with first order (Rosenkranz) line mixing coefficients [5].

There are several publications reporting the pressure-broadened half-width coefficients and pressure-induced shift coefficients for transitions of the $2\leftarrow0$ band of $^{12}C^{16}O$ (see, for example, Ref. [4] and the references therein). Comparisons of widths and shift coefficients from earlier measurements have been provided in Refs. [3,4]. Results from the present study are compared with only those that are directly applicable to the present investigation. However, it is informative to mention some of the pioneering investigations on CO. Self-, air- and CO_2-broadened half-width coefficients for several R-branch transitions in the fundamental band ($1\leftarrow0$ band of $^{12}C^{16}O$) at low temperatures were reported more than 3 decades ago by Varanasi [6]. Nakazawa and Tanaka [7] published low temperature measurements of intensities and half-width coefficients of R-branch transitions in the fundamental band of $^{12}C^{16}O$ using CO as well as N_2, O_2 and CO_2 as the broadening gases. Those authors noted that in the case of self-broadening a slight departure from the Lorentz profile started to occur even at 150 K for several strong lines. With decreasing temperature the departure from the Lorentz line profile was found to be more and more pronounced. This observation is very interesting in the context of the present study because an inexplicable behavior started to appear when spectra recorded at ~150 K were added to the least squares solution. Nakazawa and Tanaka [7] also observed that $\boldsymbol{n}$, the temperature dependence exponents for pressure-broadened half-width coefficients were different for different broadening gases and different transitions. In 1983 Bouanich [8] reported pressure-induced shifts in the first overtone band of CO broadened with CO and N_2 at 298, 193 and 133 K. From data obtained at 0.042 cm^{-1} resolution he observed that the pressure-induced shifts appeared to decrease slightly with decreasing temperature and provided calculated line shifts at ~298 K for self- and N_2-broadened CO. A year later, Bouanich et al. [9] published experimental half-width coefficients of CO lines in the $2\leftarrow0$ band at various temperatures (298, 198, 131 and 85 K) by analyzing spectra recorded at 0.042 cm^{-1} resolution. Those measurements confirmed that line widths are m-dependent ($m=-J''$ for P and $J''+1$ for R lines); but the temperature dependence exponent did not show any significant dependence on m. Some variations were observed and they concluded that there is a possibility that the temperature dependence exponent increases with m. These authors [9] presented an interesting discussion on the formation of van der Waals complexes at low temperatures which could affect the dependence of $\boldsymbol{n}$ on m. Bouanich et al. [10] later published pressure-induced line-shift coefficients in the $2\leftarrow0$ band for self-, He-, Kr-, O_2- and N_2- broadening. From data obtained with a tunable difference frequency laser spectrometer, they measured line-shift coefficients for 18 transitions (ranging between P7 and R21). The systematic errors influencing the accuracy of the measured broadening coefficients were assumed to be due to CO adsorbed on the cell wall (which is released when the foreign gas is added) and for foreign gas broadening, by the inhomogeneity in the gas mixtures. Some of those difficulties noted by previous investigators also were observed in the present study.

One of the most exhaustive recent room-temperature measurements of the self-broadened 2←0 band is by Brault et al. [4]. They reported precise room temperature values of intensities, self-broadening and self-induced pressure shift coefficients for P32 to R34 transitions using spectra recorded with the McMath-Pierce Fourier transform spectrometer located at the National Solar Observatory on Kitt Peak. The authors tested a number of Dicke-narrowed, speed-dependent profiles to assess various collisional mechanisms. By simultaneously fitting several multiline spectra, they concluded that speed-dependent broadening dominated the line shape distortions, line mixing was responsible for line asymmetries and Dicke narrowing was strongly suppressed.

In the present work 28 room- and low-temperature spectra have been fit simultaneously to determine accurate rovibrational constants, band intensities, Herman–Wallis coefficients, as well as a number of other spectral line shape parameters including widths, shifts and their temperature dependences. Line mixing coefficients were measured using the off-diagonal relaxation matrix element formalism. Temperature dependence of self-broadened line mixing was determined for the first time in any CO band. Although the temperature dependence of air-induced line mixing could not be retrieved line-by-line, it was necessary to use a default value in the least squares fit. Comparisons between self- and air-broadened half widths, self- and air-induced shifts and self- and air- line mixing coefficients from the present work are presented. Comparisons to other recent measurements [3,4] of intensities and line shape parameters are made.

A significant difference between this study and previous studies of CO is the incorporation of quantum mechanical equations for line position and intensity within the multispectrum fit of the experimental spectra over the entire spectral region (4000–4360 cm^{-1}) simultaneously in a single least squares optimization. The multispectrum fitting procedure developed by Benner et al. [11] is able to retrieve rovibrational and intensity parameters for an entire band or several bands, e.g. Ref. [12] in a single fit. Thus, a whole band analysis was performed to determine the rovibrational and band intensity values including the Herman–Wallis coefficients; individual line intensities and line positions were computed using the constants determined from the multispectrum fits. No constraints were applied to the broadening coefficients (widths, shifts, their temperature dependences, off-diagonal relaxation matrix elements) or the speed dependence. These unconstrained parameters were determined individually line-by-line. The Voigt line profile routine developed by Letchworth and Benner [13] was applied in the analysis.

By fitting a large number (28) of spectra simultaneously, the present study provides a consistent, systematic and accurate measurement for all measured parameters in the 2←0 band. Random errors in the measurements are minimized by fitting simultaneously several spectra. Nevertheless, there are still a few unresolved problems that will be discussed in the following sections.

2. Experiment

The summary of the experimental conditions is provided in Table 1. Three of the spectra are self-broadened CO previously recorded at room temperature with the McMath-Pierce FTS at Kitt Peak (for studies of the 2–0 and 3–0 CO overtones [4,14]). Briefly, a Quartz lamp served as the IR source in conjunction with a wedged CaF_2 beam splitter and two LN_2-cooled InSb detectors. Each spectrum

Table 1
Summary of experimental conditions of the CO spectra analyzed in this work.

CO				CO in air				
Temp. (K)	Pressure (Torr)	Path (m)	cv[a]	Temp. (K)	Pressure (Torr)	CO VMR	Path (m)	cv[a]
297.95	5.11	1.5 [b]	1.000000340	298.0	94.09	0.0701	0.2038	0.9999999643
297.75	401.4	1.5	1.000000330	298.0	356.32	0.1398	0.2038	0.9999999219
297.85	298.2	1.5	1.000000326	298.0	707.66	0.0707	0.2038	0.9999999206
297.35	20.23	0.2038[c]	0.9999999252	241.15	201.56	0.1375	0.2038	0.9999999222
298.00	250.78	0.2038	0.9999999253	241.65	413.89	0.0721	0.2038	0.9999999218
298.00	600.12	0.2038	0.9999999246	241.65	654.78	0.1386	0.2038	0.9999999218
298.00	712.03	0.2038	0.9999999228	191.15	148.68	0.0797	0.2038	0.9999999223
298.10[d]	20.92	0.2038	0.9999999229	191.15	300.74	0.1371	0.2038	0.9999999227
298.15[e]	20.16	0.2038	0.9999999207	191.15	513.41	0.0808	0.2038	0.9999999225
241.65	124.54	0.2038	0.9999999227	151.45	99.87	0.1389	0.2038	0.9999999329
241.15	405.97	0.2038	0.9999999198	151.15	251.07	0.0690	0.2038	0.9999999228
191.65	202.38	0.2038	0.9999999221	151.65	699.14	0.1420	0.2038	0.9999999224
191.65	504.68	0.2038	0.9999999218					
151.40	100.15	0.2038	0.9999999218					
151.15	347.88	0.2038	0.9999999216					
151.15	599.00	0.2038	0.9999999226					

[a] Wavelength calibration scaling factor (see the text for details).
[b] The three spectra with 1.5 m cell used a high-purity (99.9%) ^{12}C-enriched CO sample. 1 atm=101.3 kPa=760 Torr.
[c] All data recorded with the 20.38 cm cell used a high purity (99.5%) ^{12}C-enriched CO sample.
[d] ^{13}C-enriched (^{13}C, 99%) CO.
[e] ^{18}O-enriched (^{18}O, 98%) CO.

was recorded at 0.011 cm^{-1} resolution with ~90 min integration time and covered an optical band pass of 3650–7010 cm^{-1}. The entrance aperture to the FTS chamber was 8 mm, and the gas sample was high purity (99.9%) enriched $^{12}C^{16}O$.

The majority of the spectra (25) were recorded at 0.005 cm^{-1} resolution with the Bruker IFS 125HR Fourier transform spectrometer at JPL configured with a globar source, a CaF_2 beam splitter and a LN_2-cooled InSb detector. A coolable absorption cell with a path length of 20.38 cm was installed inside the sample compartment of the Bruker FTS and was operated at temperatures between ~298 and 150 K [15]. The cold cell was enclosed in a vacuum box to avoid icing on its wedged ZnSe windows by cryopumping residual H_2O inside the FTS; the wedged windows on the vacuum chamber were made of KBr [15]. Prior to data recording, the absorption cell was pumped for several hours to remove all residual gas contaminants including water vapor. The entire optical path within the FTS chamber was evacuated to a pressure of 0.005 Torr. For a pure sample spectrum, the cell was filled with research-grade (99.5%) CO obtained from Matheson. Spectra using the special CO samples (^{13}C-enriched (^{13}C, 99%) and ^{18}O-enriched (^{18}O, 98%)) purchased from Isotech were also recorded. The FTS was set to scan with a maximum optical path difference (MOPD) of 100 cm to achieve an unapodized spectral resolution of 0.005 cm^{-1} for all the spectra. The optical filter placed between the beam splitter and the secondary aperture restricted the bandpass to the 3550 to 5250 cm^{-1} interval; the aperture diameter was set to 1 mm. The interferograms were collected and co-added every 10 min and then individually Fourier transformed to obtain individual spectra which were then coadded. Each spectrum required approximately 3–4 h of data collection. The sample pressures were continually monitored using calibrated capacitance manometers (or Baratron pressure gauges as appropriate) with 0–10, 0–100 and 0–1000 Torr pressure ranges.

For the Bruker spectra, at each temperature, several spectra of pure CO were recorded first. Sample pressures were then increased or decreased to get the desired sets of spectra. For air-broadened spectra, pure CO sample of the required pressure was first added to the cell. Dry research grade air was then added to form volume mixing ratios of CO of 0.07–0.14 to observe both low- and high-J transitions with optimum absorption depths (50–80% absorbing). The sample temperatures were monitored throughout the spectrum recording with silicon diode temperature sensors that were attached to the cell body. For cold spectra, sufficient time was given for temperature stabilization before recording each spectrum.

The multispectrum fitting technique requires that a consistent relative calibration of the wavelength scales of all spectra be obtained before initiating retrievals. For the spectral band pass used in the analysis, this was achieved using the residual water vapor lines between 3760 and 3900 cm^{-1}, whose positions were calibrated against the $2\leftarrow0$ CO positions available from the National Institute of Standards and Technology [NIST] reference data produced by Maki and Wells [16] that are essentially the same as that published by Pollock et al. [17]. The resulting multiplicative wavenumber calibration correction factors, cv, for the spectra are listed in Table 1.

3. Data reduction and analysis

Each of the 28 experimental spectra fitted in the present study cover the entire 4000–4360 cm^{-1} spectral region of the $2\leftarrow0$ band. A consistent set of line parameters were retrieved from fitting the entire spectral range of all spectra simultaneously. The strongest features in the spectra correspond to the $2\leftarrow0$ band of $^{12}C^{16}O$. In addition to the high purity ^{12}CO spectra, two spectra, one with (99% ^{13}C-enriched) ^{13}CO and the other with (98% ^{18}O-enriched) $C^{18}O$ were also included in the solution (see Table 1) so that positions and intensities of transitions from rarer isotopologues appearing in the normal sample were precisely determined. The low-pressure room temperature pure sample spectrum was first fit. Constraints for positions and intensities were written using Eqs. (1)–(3). Low pressure ^{13}C-enriched and ^{18}O-enriched spectra were then added to the solution (constraints for rovibrational and intensity parameters were written for those bands as well). The rotational and intensity parameters were carefully adjusted in the fit until all 3 spectra were fit satisfactorily. Higher pressure room temperature self- and air-broadened spectra and the higher pressure, long path pure CO spectra were then added one at a time to the multispectrum fit. The low temperature spectra were then added, cautiously releasing the various spectral line parameters (such as the temperature dependences of widths and shifts) until all spectra were fit satisfactorily with the minimum possible residuals. Although the three CO samples with pressures of ~20 Torr were enriched with three different isotopologues (^{12}CO, ^{13}CO and $C^{18}O$), each of those samples contained various isotopologue mixtures of minor species. It was important that the amounts of each isotopologue present in each gas sample in each spectrum be determined with sufficient accuracy such that all features were fit within the noise levels of the spectra. This procedure determined the rovibrational and band intensity parameters (including Herman–Wallis factors) of the $2\leftarrow0$ band in 4 different species ($^{12}C^{16}O$, $^{13}C^{16}O$, $^{12}C^{18}O$ and $^{13}C^{18}O$). The parameters for $^{13}C^{18}O$ were less accurate due to its weak absorptions. Nevertheless, because the absorptions due to isotopologues other than the major species are rather small in a given sample, the rovibrational and intensity parameters retrieved were best determined from spectra obtained with the particular isotopologue as the major species. It is also possible that when a specific CO sample is cooled or diluted with air, the isotopologue enrichment of the minor species could be preferentially depleted or enhanced due to adsorption on the cell wall (thus differing from the manufacturer's specifications) but must be determined sufficiently precisely for minimizing the fit residuals. Such a multispectrum fit brings internal physical consistency across all the fitted spectra. As noted in [12] by fitting an entire band all at once rather than fitting a few lines at a time (or even fitting a set of spectra with limited wavenumber range recorded at one temperature

simultaneously) errors arising from experimental measurement sources such as the zero level (100% transmittance) and residual FTS phase errors are minimized. Similarly, determining the best value for the volume mixing ratio of the absorbing gas in a foreign-broadened spectrum that fits the entire spectral range was both time consuming and challenging; but highly important to reduce systematic errors. Using one continuous background polynomial fit for each fitted spectrum reduced the correlation between intensity and broadening parameters because the same solution must work for all spectra analyzed under all measurement conditions (e.g. pressure, temperature and path length) and forced the physical requirement that the 100% transmittance level be continuous.

Eqs. (1)–(3) were used to solve for the rovibrational (G, B, D, H…) and transition moment constants (vibrational band strength S_ν, and the Herman–Wallis type coefficients a_1, a_2, a_3 and a_4) for the $2\leftarrow 0$ band rather than the individual line positions, ν_i, and intensities, S_i, at 296 K:

$$\nu_i = G'-G''+(B'J'[J'+1]-D'\{J'[J'+1]\}^2+H'\{J'[J'+1]\}^3) \\ -(B''J''[J''+1]-D''\{J''[J''+1]\}^2+H''\{J''[J''+1]\}^3) \quad (1)$$

$$S_i(T_0) = \frac{S_\nu \nu_i L_i F}{Q_r \nu_0} exp\left(\frac{-C_2 E''}{T_0}\right)\left[1-exp\left(\frac{-C_2 \nu_i}{T_0}\right)\right] \quad (2)$$

where

$$F = 1+a_1 m+a_2 m^2+a_3 m^3+a_4 J(J+1) \quad (3)$$

In the present study it was found that the a_1, a_2 and a_3 terms were sufficient to describe the band to the noise level of the spectra. The a_4 term was not used and only retained in the expression for the sake of completeness. ν_i is the transition wavenumber (cm^{-1}) of the ith line, prime and double prime refer to the upper and lower vibrational levels, respectively. In Eq. (2), L_i are the Hönl–London factors and C_2 represents the second radiation constant; J is the rotational quantum number, Q_r the rotational quantum partition function, ν_0 the band center (equal to G'–G''), E'' is the lower state energy and T_0 is the reference temperature (296 K here). The value of Q_r used in the present study was 107.1134 [2]; Brault et al. [4] assumed a value of 107.417 while Zou and Varanasi [3] did not provide the value used in their measurements.

The number of adjusted parameters in the present study was reduced by fitting several spectra simultaneously. The pressure-induced shifts were better determined because of the more precise zero-pressure line position retrievals and the reduction of correlation between the zero-pressure line positions and the pressure-induced shifts. Correlations were also reduced between line intensities and the Lorentz half widths which are characteristics for strong lines. This correlation was minimized by constraining the line intensity of each spectral line to be consistent with the rest of the lines in the band.

Minor effects on spectral line shapes (such as speed dependence, Dicke narrowing) become increasingly important especially when the least squares fits fail to converge even with high-quality spectra in the solution. Dicke (collisional) narrowing must usually be considered in fitting low pressure spectra (20 Torr in this case) where the Doppler contribution is significant compared to the Lorentz width. The effects of collisional narrowing can be neglected at higher pressures where the Doppler contribution is small compared to the Lorentz width.

When only the 3 low pressure spectra (20 Torr) of high purity ^{12}CO, ^{13}CO and $C^{18}O$ samples were initially fit (see Table 1), Dicke narrowing was found significant to reduce the fitted residuals. The measured Dicke narrowing was found to be transition dependent. When higher pressure spectra were added to the fit, Dicke narrowing was inadequate to remove the residuals and speed-dependent parameter became more important than Dicke narrowing. When both Dicke narrowing and speed dependence parameters were simultaneously adjusted in the fit, the fit became unstable and slowly diverged. A similar observation was made by Brault et al. [4] stating that the Dicke narrowing and speed-dependence parameters were strongly influenced by the particular model chosen. Further, Brault et al. [4] noted that in fitting certain spectra, they were unable to determine the relative influence of Dicke narrowing and speed dependence. From their high quality fits using the speed-dependent Voigt and also the very small diffusion coefficient with the speed-dependent Rautian model, they observed that for self-broadened CO, Dicke narrowing was strongly suppressed and the deviations from the conventional Voigt were primarily due to speed-dependent broadening. Dicke narrowing was difficult to measure on our spectra since the Doppler half width of the CO lines ($<0.005\ cm^{-1}$) is at best only about equal to the resolution of the spectra and little shape information was available.

To reduce the residuals further, the widths and shift coefficients and their temperature dependences were adjusted. The residuals characteristic of line mixing were reduced by including the off-diagonal relaxation matrix element coefficients for both the self- and air- line mixing. It was possible to adjust the temperature dependences of self-line mixing for the strong transitions, but for air-induced line mixing only a default constant temperature-dependence exponent of 0.7 could be included for each mixed pair of transitions. The optical densities of CO in the air-broadened spectra were not high enough to measure the values for each pair independently and reliably from the present dataset.

The multispectrum fit of all the 28 spectra is shown in Fig. 1. The top panel (a) shows all 28 experimental spectra and panel (b) shows the weighted observed minus calculated fit residuals on an expanded vertical scale. In assigning weights, a maximum weight of 1.0 was given to the best signal-to-noise spectrum (several spectra were given weights of 1.0 in this study) and adjusted the weighted contributions of other spectra based upon their respective signal-to-noise.

The weighted fit residuals arising from specific sets of spectra (obtained from the multispectrum fit) are plotted separately in the lower panels (c–e) of Fig. 1. Even after taking into account all critical spectral line parameters including line mixing, speed dependence and instrument effects such as field of view into the least squares fit, some

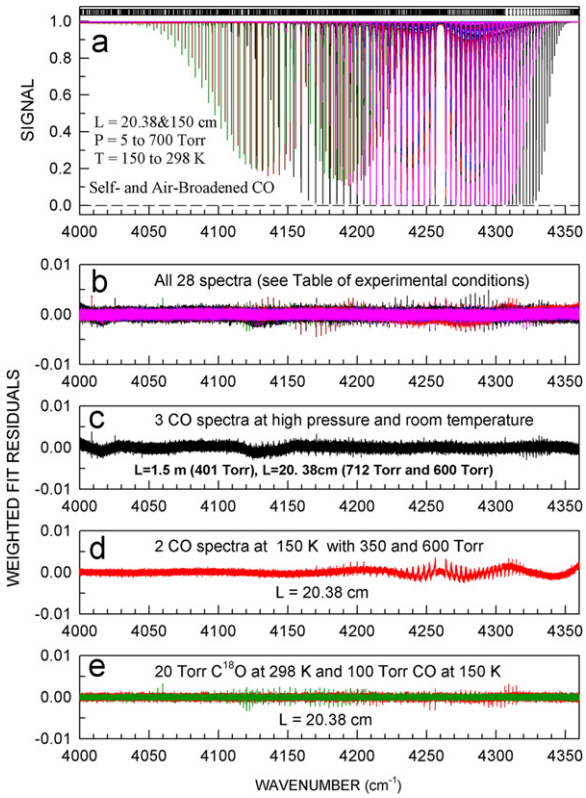

Fig. 1. Multispectrum fit of CO spectra in the 4000 to 4360 cm^{-1} region. (a) Twenty eight experimental spectra (16 self-broadened and 12 air-broadened) are overlaid. The 100% absorption line is shown by the dashed horizontal line at the bottom of (a). The vertical tick marks at the top of (a) correspond to positions of ~1000 lines included in the fit. Color codes: black (~298 K); pink (~240 K); blue (~190 K); red (~150 K); dark red (^{13}CO at ~298 K) and dark green ($C^{18}O$ at ~298 K). The same color codes are used for both the self- and the air-broadened spectra recorded at similar temperatures (see Table 1). The weighted fit residuals (observed minus calculated) on an expanded vertical scale are plotted in panel (b). Panels (c)–(e) show weighted fit residuals from various subsets of the spectra. (c) The residuals near 4050 and 4150 cm^{-1} may be due to unidentified impurities (e.g. nickel carbonyl) in the sample. (d) These residuals may be due to collision-induced absorption or may indicate failure of the line shape modeling at 150 K. (e) These sharp residuals mostly appear in low pressure spectra where Dicke narrowing is most important. Some of these residuals could be caused by unaccounted instrumental line shape effects. It must be emphasized that the residuals plotted in each panel (c–e) are from the multispectrum fit and not from fitting the few spectra identified in the respective panels. (For interpretation of the references to color in this figure legend, the reader is referred to the web version of this article.)

residuals were still present. These residuals were persistent and thought to be due to absorptions caused by some unknown impurities in the samples, such as nickel carbonyl (broad features near 4050 and 4130 cm^{-1}) seen in the P-branch side of the high-pressure self-broadened spectra shown in panel (c) or by collision-induced absorptions (CIA) as seen in panel (d) or other types of residuals that are rather sharp and narrow which may be attributed to unaccounted portion of the instrument line shape as plotted in panel (e). Pure sample spectra at the lowest temperature and higher pressures showed features (d) that could not be removed in spite of adjusting all spectral line parameters. The multispectrum fitting technique took into account the small ($\leq 1\%$) contribution due to van der Waals correction to the perfect gas law. The dashed horizontal line drawn at the bottom portion of panel (a) in Fig. 1 corresponds to 100% absorption. The short vertical lines at the top of panel (a) indicate positions of individual lines included in the fit. 19 of the 28 spectra required only a first or a second degree polynomial to fit the spectrum background while a 6th–7th degree polynomial was needed to fit the background for 6 out of the 7 remaining spectra (the spectra recorded at 150, 190 K and the 2 highest pressure room temperature spectra with 20.38 cm long cell). One spectrum taken at room temperature with the 1.5 m cell required a 4th degree polynomial to fit its background. Increasing the degree of polynomial did not remove the residuals seen in Fig. 1d. The reason for these remaining residuals is not known.

4. Results

The spectral line parameters determined from the present study are listed in Tables 2 and 3. Although line positions and intensities for this band have been reported in many prior studies, it is important that a consistent set of all line parameters be used in any precise atmospheric retrieval. For that reason line positions and intensities determined in this study are also provided along with other measured parameters. Even though both self- and air-broadened spectra were fit together and all line parameters were determined from a single multispectrum fit, for convenience, the results for self- and air-broadening are given separately. Table 2 lists the parameters for self-broadening and Table 3 provides values for air-broadening. These tables contain the rotational quantum identification, the calculated zero-pressure line center positions (ν in cm^{-1}), calculated line intensity (cm^{-1}/(molecule cm^{-2}) at 296 K), the measured Lorentz broadening coefficients b_L^0 in $cm^{-1}\,atm^{-1}$ at 296 K, their temperature dependence exponents n (unitless), pressure-induced shift coefficients δ^0 in $cm^{-1}\,atm^{-1}$ at 296 K and their temperature dependence coefficient δ' in $cm^{-1}\,atm^{-1}\,K^{-1}$. Only a single speed-dependent parameter was determined for each transition appropriate to both self- and air-broadening and these are listed with their uncertainties in Table 2. The uncertainties in the retrieved parameters are listed adjacent to their measured values and correspond to one standard deviation in the measured quantity as determined by the fit, but not including systematic effects due primarily to uncertainties in the physical parameters of the gas conditions for each spectrum.

The retrieved rovibrational (G, B, D, H…) and intensity (band strength S_ν, and Herman–Wallis coefficients a_1, a_2, a_3) parameters are listed in Table 4. This table also provides the correlation coefficients between appropriate pairs of the fitted parameters. These correlation coefficients are required to compute the uncertainties in line positions and intensities (not listed in Table 2 but shown in Figs. 2 and 4) of individual lines. These values provide confidence in the present multispectrum solution. Positions and intensities for only those transitions observed in

Table 2
Self-broadened line parameters for the 2←0 band of $^{12}C^{16}O$.

Line	Position[a]	Intensity[b]	b_L^0 (self)[c]	%unc.	n (self)	%unc.	δ^0 (self)[d]	Unc.	δ' (self)[e]	unc.[f]	SD[g]	%unc.[f]
P29	4120.728522	5.2048E-22	0.04592	0.37								
P28	4126.474269	8.6559E-22	0.04704	0.28			-0.00546	(15)	0.0000000	(F)	0.070	(F)
P27	4132.154100	1.4116E-21	0.04811	0.19			-0.00522	(10)	0.0000000	(F)	0.070	(F)
P26	4137.767872	2.2570E-21	0.04908	0.20			-0.00533	(7)	0.0000000	(F)	0.076	10.0
P25	4143.315439	3.5378E-21	0.04997	0.14			-0.00541	(7)	0.0000000	(F)	0.079	6.8
P24	4148.796658	5.4356E-21	0.05101	0.10	0.7062	1.84	-0.00533	(4)	0.0000347	(32)	0.083	4.7
P23	4154.211383	8.1850E-21	0.05174	0.08	0.7066	1.09	-0.00533	(3)	0.0000329	(19)	0.071	4.5
P22	4159.559471	1.2077E-20	0.05264	0.06	0.7161	0.66	-0.00525	(3)	0.0000321	(12)	0.066	3.9
P21	4164.840774	1.7458E-20	0.05373	0.06	0.7097	0.42	-0.00534	(2)	0.0000291	(8)	0.070	2.7
P20	4170.055148	2.4719E-20	0.05473	0.04	0.7114	0.27	-0.00524	(2)	0.0000280	(5)	0.064	2.5
P19	4175.202448	3.4272E-20	0.05584	0.04	0.7107	0.18	-0.00531	(2)	0.0000261	(4)	0.070	1.8
P18	4180.282527	4.6517E-20	0.05692	0.04	0.7140	0.13	-0.00523	(1)	0.0000257	(3)	0.070	1.5
P17	4185.295239	6.1788E-20	0.05801	0.02	0.7171	0.10	-0.00519	(1)	0.0000258	(2)	0.071	1.3
P16	4190.240438	8.0288E-20	0.05900	0.02	0.7211	0.07	-0.00507	(1)	0.0000252	(2)	0.068	1.2
P15	4195.117977	1.0201E-19	0.06010	0.02	0.7249	0.07	-0.00505	(1)	0.0000247	(1)	0.074	1.0
P14	4199.927711	1.2666E-19	0.06106	0.02	0.7279	0.06	-0.00505	(1)	0.0000233	(1)	0.070	1.0
P13	4204.669493	1.5359E-19	0.06205	0.02	0.7316	0.06	-0.00505	(1)	0.0000230	(1)	0.073	0.9
P12	4209.343176	1.8173E-19	0.06295	0.02	0.7364	0.04	-0.00487	(1)	0.0000224	(1)	0.074	0.8
P11	4213.948613	2.0960E-19	0.06383	0.02	0.7424	0.04	-0.00479	(1)	0.0000220	(1)	0.077	0.8
P10	4218.485657	2.3533E-19	0.06471	0.02	0.7481	0.04	-0.00465	(1)	0.0000227	(1)	0.078	0.7
P9	4222.954162	2.5676E-19	0.06564	0.02	0.7533	0.03	-0.00454	(1)	0.0000231	(1)	0.085	0.6
P8	4227.353981	2.7158E-19	0.06671	0.02	0.7533	0.03	-0.00445	(1)	0.0000221	(1)	0.087	0.6
P7	4231.684966	2.7754E-19	0.06807	0.01	0.7507	0.03	-0.00430	(1)	0.0000213	(1)	0.096	0.5
P6	4235.946971	2.7272E-19	0.06986	0.01	0.7457	0.03	-0.00413	(1)	0.0000198	(2)	0.103	0.4
P5	4240.139848	2.5573E-19	0.07216	0.01	0.7410	0.03	-0.00388	(1)	0.0000175	(2)	0.107	0.4
P4	4244.263451	2.2595E-19	0.07494	0.01	0.7396	0.03	-0.00355	(1)	0.0000133	(2)	0.109	0.4
P3	4248.317633	1.8371E-19	0.07821	0.01	0.7417	0.03	-0.00320	(1)	0.0000102	(2)	0.107	0.4
P2	4252.302246	1.3031E-19	0.08218	0.01	0.7449	0.04	-0.00290	(1)	0.0000081	(2)	0.104	0.4
P1	4256.217143	6.8044E-20	0.08782	0.02	0.7447	0.05	-0.00259	(2)	0.0000062	(2)	0.107	0.4
R0	4263.837202	7.0173E-20	0.08792	0.02	0.7473	0.05	-0.00287	(1)	0.0000080	(2)	0.106	0.4
R1	4267.542071	1.3859E-19	0.08241	0.01	0.7469	0.04	-0.00332	(1)	0.0000124	(2)	0.105	0.4
R2	4271.176636	2.0149E-19	0.07838	0.01	0.7413	0.03	-0.00362	(1)	0.0000155	(2)	0.111	0.4
R3	4274.740751	2.5557E-19	0.07501	0.01	0.7375	0.03	-0.00378	(1)	0.0000152	(2)	0.117	0.3
R4	4278.234269	2.9829E-19	0.07207	0.01	0.7391	0.03	-0.00383	(1)	0.0000146	(2)	0.116	0.4
R5	4281.657043	3.2804E-19	0.06966	0.01	0.7424	0.03	-0.00387	(1)	0.0000145	(2)	0.112	0.4
R6	4285.008927	3.4426E-19	0.06778	0.01	0.7473	0.03	-0.00393	(1)	0.0000129	(2)	0.106	0.4
R7	4288.289774	3.4736E-19	0.06632	0.02	0.7509	0.03	-0.00399	(1)	0.0000128	(2)	0.098	0.5
R8	4291.499438	3.3865E-19	0.06521	0.02	0.7495	0.03	-0.00398	(1)	0.0000128	(2)	0.093	0.5
R9	4294.637772	3.2005E-19	0.06422	0.02	0.7462	0.03	-0.00398	(1)	0.0000147	(1)	0.088	0.6
R10	4297.704629	2.9391E-19	0.06335	0.02	0.7393	0.03	-0.00401	(1)	0.0000162	(1)	0.084	0.7
R11	4300.699864	2.6274E-19	0.06248	0.02	0.7296	0.04	-0.00401	(1)	0.0000181	(1)	0.080	0.7
R12	4303.623331	2.2894E-19	0.06158	0.02	0.7207	0.04	-0.00405	(1)	0.0000201	(1)	0.077	0.8
R13	4306.474883	1.9464E-19	0.06067	0.02	0.7125	0.04	-0.00414	(1)	0.0000209	(1)	0.076	0.8
R14	4309.254374	1.6161E-19	0.05972	0.02	0.7103	0.06	-0.00428	(1)	0.0000215	(1)	0.077	0.8
R15	4311.961659	1.3112E-19	0.05874	0.02	0.7085	0.06	-0.00444	(1)	0.0000221	(1)	0.077	0.9
R16	4314.596591	1.0402E-19	0.05772	0.02	0.7069	0.07	-0.00459	(1)	0.0000228	(1)	0.075	1.0
R17	4317.159026	8.0715E-20	0.05667	0.02	0.7050	0.09	-0.00473	(1)	0.0000236	(1)	0.076	1.0
R18	4319.648816	6.1292E-20	0.05563	0.02	0.7034	0.11	-0.00489	(1)	0.0000248	(2)	0.073	1.3
R19	4322.065818	4.5560E-20	0.05456	0.02	0.6990	0.16	-0.00508	(1)	0.0000251	(2)	0.074	1.4
R20	4324.409885	3.3160E-20	0.05344	0.04	0.7047	0.21	-0.00523	(2)	0.0000258	(4)	0.072	1.8
R21	4326.680872	2.3638E-20	0.05241	0.04	0.6994	0.33	-0.00534	(2)	0.0000277	(6)	0.069	2.3
R22	4328.878633	1.6507E-20	0.05138	0.06	0.7020	0.50	-0.00545	(2)	0.0000295	(9)	0.069	2.9
R23	4331.003025	1.1295E-20	0.05035	0.06	0.6976	0.82	-0.00554	(2)	0.0000337	(14)	0.065	4.0
R24	4333.053901	7.5733E-21	0.04932	0.08	0.7059	1.33	-0.00572	(4)	0.0000343	(22)	0.060	5.6
R25	4335.031116	4.9771E-21	0.04847	0.12			-0.00587	(5)	0.0000000	(F)	0.069	6.3
R26	4336.934526	3.2063E-21	0.04746	0.15			-0.00601	(5)	0.0000000	(F)	0.068	8.8
R27	4338.763986	2.0250E-21	0.04665	0.21			-0.00612	(7)	0.0000000	(F)	0.071	11.8
R28	4340.519350	1.2540E-21	0.04564	0.20			-0.00643	(10)	0.0000000	(F)	0.060	(F)
R29	4342.200475	7.6149E-22	0.04462	0.31			-0.00636	(16)	0.0000000	(F)	0.060	(F)
R30	4343.807215	4.5348E-22	0.04337	0.48			-0.00702	(24)	0.0000000	(F)	0.060	(F)

[a] Zero pressure line positions in cm^{-1}. The line positions are calculated using the rovibrational constants listed in Table 4. Refer to Fig. 2 and Eq. (4) for the position uncertainties.

[b] Line intensities are in cm^{-1}/(molecule cm^{-2}) at 296 K. Intensities are for $^{12}C^{16}O$ fraction in a natural CO sample (0.986433). The listed intensities are values calculated using the vibrational band intensity and the Herman–Wallis parameters listed in Table 4. Refer to Fig. 2 and Eq. (4) for intensity uncertainties.

[c] The measured Lorentz half-width coefficients are in cm^{-1} atm^{-1} at 296 K.

[d] The measured pressure-induced shift coefficients are in cm^{-1} atm^{-1} at 296 K.

[e] The measured temperature dependence of pressure-induced shift coefficients are in cm^{-1} atm^{-1} K^{-1}.

[f] *F* indicates the values are fixed.

[g] Speed-dependence parameter (unitless). Both self- and air-broadening are assumed to have the same value.

Table 3
Air-broadened line parameters[a] for the 2←0 band of $^{12}C^{16}O$.

Line	b_L^0 (air)[b]	%unc.	n (air)	%unc.	δ^0 (air)[c]	unc.	δ' (air)[d]	unc[e].
P23	0.04843	0.48			-0.00559	(9)	0.0000000	(F)
P22	0.04914	0.31			-0.00508	(8)	0.0000000	(F)
P21	0.05019	0.22			-0.00594	(6)	0.0000000	(F)
P20	0.05031	0.18	0.7424	1.56	-0.00546	(6)	0.0000151	(10)
P19	0.05134	0.14	0.7369	1.03	-0.00535	(5)	0.0000196	(10)
P18	0.05194	0.10	0.7587	0.66	-0.00531	(4)	0.0000212	(7)
P17	0.05294	0.08	0.7558	0.45	-0.00522	(4)	0.0000232	(6)
P16	0.05364	0.06	0.7607	0.30	-0.00523	(3)	0.0000237	(5)
P15	0.05453	0.06	0.7649	0.22	-0.00511	(3)	0.0000250	(4)
P14	0.05522	0.04	0.7697	0.16	-0.00505	(2)	0.0000248	(5)
P13	0.05593	0.04	0.7753	0.13	-0.00493	(2)	0.0000256	(3)
P12	0.05660	0.04	0.7809	0.10	-0.00495	(2)	0.0000247	(2)
P11	0.05731	0.03	0.7850	0.09	-0.00488	(2)	0.0000250	(2)
P10	0.05793	0.03	0.7901	0.08	-0.00484	(1)	0.0000249	(2)
P9	0.05869	0.03	0.7909	0.08	-0.00477	(1)	0.0000243	(2)
P8	0.05955	0.03	0.7886	0.06	-0.00469	(1)	0.0000237	(2)
P7	0.06078	0.03	0.7826	0.06	-0.00460	(1)	0.0000234	(2)
P6	0.06261	0.03	0.7721	0.06	-0.00444	(1)	0.0000230	(2)
P5	0.06487	0.03	0.7619	0.07	-0.00419	(1)	0.0000219	(2)
P4	0.06787	0.03	0.7588	0.07	-0.00380	(2)	0.0000193	(2)
P3	0.07130	0.03	0.7657	0.08	-0.00329	(2)	0.0000159	(2)
P2	0.07518	0.04	0.7745	0.08	-0.00298	(2)	0.0000128	(3)
P1	0.08046	0.06	0.7815	0.14	-0.00279	(4)	0.0000118	(4)
R0	0.08040	0.06	0.7815	0.13	-0.00332	(4)	0.0000072	(4)
R1	0.07525	0.04	0.7752	0.08	-0.00360	(2)	0.0000108	(2)
R2	0.07133	0.03	0.7655	0.07	-0.00375	(2)	0.0000133	(2)
R3	0.06788	0.03	0.7596	0.07	-0.00385	(1)	0.0000148	(2)
R4	0.06483	0.03	0.7617	0.07	-0.00386	(1)	0.0000160	(2)
R5	0.06240	0.03	0.7714	0.06	-0.00389	(1)	0.0000167	(1)
R6	0.06072	0.03	0.7783	0.06	-0.00391	(1)	0.0000165	(1)
R7	0.05945	0.02	0.7852	0.06	-0.00391	(1)	0.0000164	(1)
R8	0.05850	0.02	0.7875	0.06	-0.00387	(1)	0.0000168	(1)
R9	0.05777	0.03	0.7848	0.06	-0.00386	(1)	0.0000168	(1)
R10	0.05708	0.04	0.7802	0.06	-0.00384	(1)	0.0000178	(2)
R11	0.05644	0.04	0.7734	0.08	-0.00385	(1)	0.0000188	(2)
R12	0.05571	0.04	0.7693	0.09	-0.00392	(1)	0.0000194	(2)
R13	0.05502	0.04	0.7634	0.10	-0.00404	(2)	0.0000203	(2)
R14	0.05424	0.04	0.7591	0.13	-0.00413	(2)	0.0000214	(3)
R15	0.05349	0.04	0.7524	0.17	-0.00424	(2)	0.0000220	(3)
R16	0.05262	0.06	0.7520	0.24	-0.00450	(2)	0.0000215	(4)
R17	0.05184	0.06	0.7455	0.35	-0.00451	(3)	0.0000241	(5)
R18	0.05101	0.08	0.7420	0.53	-0.00475	(3)	0.0000214	(6)
R19	0.05017	0.10	0.7280	0.78	-0.00491	(4)	0.0000228	(8)
R20	0.04947	0.14	0.7451	1.17	-0.00495	(5)	0.0000143	(10)
R21	0.04878	0.16			-0.00570	(5)	0.0000000	(F)
R22	0.04752	0.23			-0.00548	(6)	0.0000000	(F)
R23	0.04658	0.34			-0.00595	(8)	0.0000000	(F)

[a] Zero pressure line positions, line intensities and speed dependence parameters are the same as in Table 2 and hence are not repeated in this table.
[b] The measured Lorentz half-width coefficients are in cm^{-1} atm^{-1} at 296 K.
[c] The measured pressure-induced shift coefficients are in cm^{-1} atm^{-1} at 296 K.
[d] The measured temperature dependence of pressure-induced shift coefficients are in cm^{-1} atm^{-1} K^{-1}.
[e] *F* indicates the values are fixed.

the spectra were included in Tables 2 and 3. The line positions and intensities can be extrapolated to higher *J* from the rovibrational and intensity parameters listed in Table 4.

The uncertainty of a constrained parameter of the solution is given in Eq.(4) as follows:

$$\varepsilon_Q^2 = \sum_{i=1}^{N} \left(\frac{\partial Q}{\partial q_i}\right)^2 \varepsilon_{q_i}^2 - 2\sum_{i=1}^{N-1}\sum_{j=i+1}^{N} \rho_{q_i q_j} \left(\frac{\partial Q}{\partial q_i}\right)\left(\frac{\partial Q}{\partial q_j}\right) \varepsilon_{q_i}\varepsilon_{q_i} \quad (4)$$

In Eq. (4), Q is the constrained parameter whose uncertainty is sought and q_i the unconstrained parameters of the solution. The uncertainty of each measured parameter is denoted by ε with the appropriate subscript and the correlation between two unconstrained parameters is denoted by ρ with an appropriate double subscript; N is the number of unconstrained parameters in the solution. The positions are constrained with Eq. (1), so the uncertainties in the constrained positions are given by substituting G' for q_1, B' for q_2, D' for q_3, H' for q_4, B'' for q_5, D'' for q_6 and H'' for q_7. For all other parameters of the solution, the appropriate derivative is zero and the related terms are zero. The derivatives are found by partial differentiation of Eq. (1).

Table 4
Rovibrational and band intensity parameters and correlation coefficients determined for the $2\leftarrow 0$ band of $^{12}C^{16}O$.

Rotational parameter	Rotational constants (cm^{-1})	Intensity parameter	Intensity constants
$G'-G''$	4260.0621764(9)	S_ν[a]	$7.47326(5)\times 10^{-20}$
B'	1.887524802(59)	a_1	$+0.516741(94)\times 10^{-2}$
D'	$0.612227(23)\times 10^{-5}$	a_2	$+0.35244(67)\times 10^{-4}$
H'	$0.933(27)\times 10^{-11}$	a_3	$-1.063(51)\times 10^{-7}$
B''	1.922529582(60)		
D''	$0.612387(25)\times 10^{-5}$		
H''	$0.991(30)\times 10^{-11}$		
Rotational parameters	**Correlation**	**Intensity parameters**	**Correlation**
$G'-G''$ and B'	+0.14049727	S_ν and a_1	−0.14334053
$G'-G''$ and D'	+0.12585014	S_ν and a_2	−0.70616204
$G'-G''$ and H'	+0.09651142	S_ν and a_3	+0.10997576
B' and D'	+0.89268547	a_1 and a_2	+0.07081920
$B'$and H'	+0.73415411	a_1 and a_3	−0.80373162
D' and H'	+0.93585435	a_2 and a_3	−0.13851970
$G'-G''$ and B''	−0.09262139		
$G'-G''$ and D''	−0.08382708		
$G'-G''$ and H''	−0.07297546		
B'' and D''	+0.89208649		
B'' and H''	+0.73195133		
D'' and H''	+0.93438017		
B' and B''	+0.95605568		
B' and D''	+0.84171174		
B' and H''	+0.68884155		
D' and B''	+0.84898043		
D' and D''	+0.94292802		
D' and H''	+0.88081525		
H' and B''	+0.69363293		
H' and D''	+0.87856418		
H' and H''	+0.94081609		

The intensities are scaled to the natural CO abundance. The rotational partition function used for $^{12}C^{16}O$ at 296 K=107.1169 [2].
[a] In units of cm/molecule at 296 K.

Table 4 provides the uncertainties in each required unconstrained parameter and the correlations between those parameters. The uncertainty in position is a function of J' and J'' that is not limited to the spectral lines that contributed significantly to the solution, but can be extrapolated and even interpolated to physically forbidden noninteger values of the quantum numbers. These relative uncertainties as a function of m ($m=-J''$ for P branch and $J''+1$ for R branch) are displayed in Fig. 2.

These uncertainties are less than $2\times 10^{-6}\,cm^{-1}$ for transitions with $m\leq 20$, less than $2\times 10^{-5}\,cm^{-1}$ for transitions with $m\leq 30$ and less than $2\times 10^{-4}\,cm^{-1}$ for transitions with $m\leq 40$. The extrapolation of the uncertainties beyond the range of observed transitions in the fitted spectra (roughly P30 to R30) is only an estimate with the assumption that there are no perturbations (a good assumption in CO) and no higher order terms become important. In Fig. 2a, we have compared the position uncertainties from this study and the absolute uncertainties of Refs. [16,17]. The precision in line positions from the present work is a few times better than the accuracy in positions from Refs. [16,17]. The absolute uncertainties are the same as in Refs. [16,17] since the retrieved line positions were normalized to their absolute line positions. In Fig. 2b we have plotted the normalized position differences between the present study and those in Refs. [16,17] vs. m (P20–R20 transitions listed in Refs. [16,17] were used for calibrating the wavenumber scales of the present data). As displayed in Fig. 2b the positions are consistent at the level of the uncertainties in each study (this study and Refs. [16,17]). The small undulations observed in Fig. 2b could be arising from various sources, such as the uncertainties in the retrieved upper and lower rovibrational constants, the limitations in the model used in fitting the data, unaccounted portion of the phase errors in the spectra fitted. Nevertheless, most of the differences are close to zero, as they should be and are indicated by the solid horizontal line.

The position uncertainties for lines with $J''>30$ are not strongly constrained by our solution. The rovibrational model is likely to require another term (such as L) before $J''=50$ where this graph ends. We are aware of only one prior laboratory measurements by Rank et al. [18] who have observed CO transitions with J values up to 48 for the $2\leftarrow 0$ band using a heated absorption cell. Our spectra do not display absorptions for lines with J'' greater than 30. In addition to the Rank et al. [18] measurements, the only way to test our uncertainties is to compare the values determined from the solar spectrum. Our constants predict that the R Branch has a band head very close to R51. The band head is clearly visible in the spectrum of the sun and the band head is roughly about $0.2\,cm^{-1}$ different from the predicted value [19,20]. From the present study the calculated uncertainty of the R51 line is about two orders of magnitude smaller than this difference. At this point the upper energy state is more

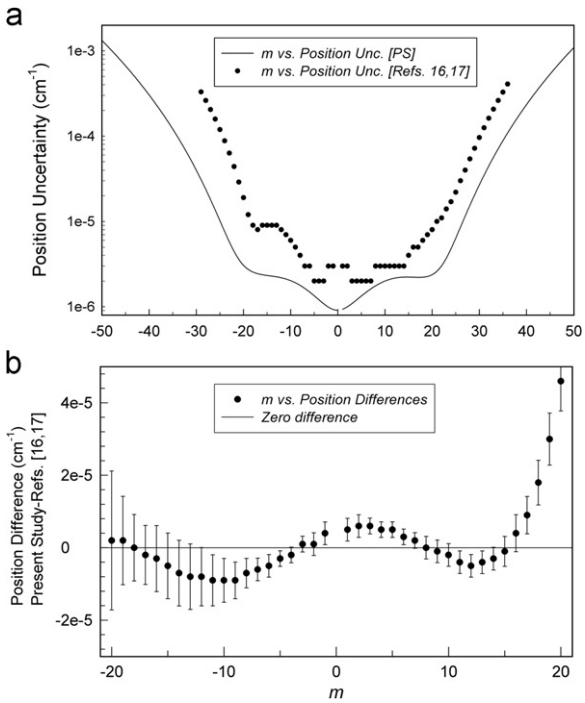

Fig. 2. (a) Position uncertainties (cm^{-1}) vs. m ($m=-J''$ for P-branch and $J''+1$ for R-branch transitions) in the $2\leftarrow 0$ band of $^{12}C^{16}O$. The position uncertainties are extended to higher m (-50 to 50) than actually observed (-30 to 30) in the spectra. This was possible since the line positions and uncertainties followed the theoretical quantum mechanical expressions. The absolute uncertainties determined by Pollock et al. [17] are plotted as points for comparison. The precision obtained from multispectrum fits is a few times better than the absolute uncertainties in [16,17]. See the text for details. (b) The position differences from present study and Ref. [17] vs. m are plotted. The range in m (-20 to $+21$) plotted in the graph corresponds to CO transitions listed in [16,17] used for wavenumber calibration of the present spectra. The horizontal solid line corresponds to zero difference between present study and Refs. [16,17].

than 9000 cm^{-1} where there are likely to be deviations from the model used here. This forms a realistic limit on how much larger the real uncertainties are compared to those calculated from our fit.

As another check to validate the accuracy of our predicted line positions for transitions beyond those observed in our data, we have compared our calculated line positions using our retrieved rovibrational constants for several transitions (for J'' that were both observed as well as extrapolated) to the calculated line positions provided in the HITRAN08 database [2] and a recent line list from Hase et al. [21]. This comparison is shown in Table 5. The line list from [21] is available online as the supplementary data associated with their article. The calculated line positions in [2] are based upon the improved Dunham coefficients for CO determined from measurements of infrared solar lines by Farrenq et al. [22]. Those Dunham coefficients were obtained from measurements of solar CO lines recorded by the ATMOS Fourier transform spectrometer. CO transitions up to $J=110$ for the first overtone band were observed in those solar spectra and measured by [22]. The positions of those CO lines were calibrated against the same wavenumber standards used in this work [17]. The line positions listed by Hase et al. [21] were also observed in solar spectra but recorded by the ACE-FTS about two decades later than the ATMOS-FTS. As seen in Table 5 the values are all in good agreement with each other within the precision reported in each of those studies. Our predicted line positions for P45 and R45 as examples are within ± 0.005 cm^{-1} from Rank et al. [18], HITRAN08 [2,22] and Hase et al. [21] values. The means and the standard deviations for the select number of transitions (Table 5) between present study with the 4 other lists compared are: (PS-Refs. [16,17])$=+0.00018(40)$ cm^{-1}; (PS-HITRAN08 [2,22])$=+0.0001(24)$ cm^{-1}, (PS-Hase et al. [21])$=+0.001(2)$ cm^{-1} and (PS-Rank et al. [18])$=+0.0021(24)$ cm^{-1}.

In retrospect, we could have constrained the lower state rotational constants to those obtained from microwave studies that were already available. However, the upper and lower state rovibrational constants are highly correlated in our least squares solution and their values can adjust in a manner that makes the rovibrational constants not quite correct, but still produce accurate positions when adequate data are available, such as in the present study.

Part of the power of our technique is that we are determining functional forms for the positions and, within the limits of the functions used, this provides some rough information on how fast the extrapolation becomes useless if the function continues to adequately represent the positions and intensities. One must also keep in mind that positions, in particular, are not a priority in the results of this paper. The emphasis is upon the line shape parameters, but the positions and intensities need to be consistently and reliably determined in order to obtain the best measurements of the other parameters and to provide a consistent set of parameters whose systematic errors tend to cancel within the physical constraints of the input data.

4.1. Intensities

The retrieved line intensities from present study using the constraint technique were found to be consistent with values in HITRAN04 [1] and HITRAN08 [2]. There have been no updates for any CO line parameters since HITRAN04 [1] and the line intensities in the HITRAN08 [2] are essentially the same as those of Brault et al. [4].

Comparisons of line intensities among this work, HITRAN08 [2] and Zou and Varanasi [3], are shown in Fig. 3. It is evident that the present intensity measurements compare better with the HITRAN08 database [2] and hence with the measurements of Brault et al. [4] than those of Zou and Varanasi [3]. The means and standard deviations of the ratios of the present intensities to those studies are 1.004(1) and 0.99(1), respectively. The differences, especially for $0\leq m\leq 10$ transitions, seen between the present study and Zou and Varanasi [3] may be attributed to the neglect of line mixing in [3]. Line intensities retrieved using the Rosenkranz line mixing [5] used in [4] and the full line mixing using the off-diagonal relaxation matrix elements [23] in the present

Table 5
Comparisons of line positions from present study to values from Pollock et al./NIST [16,17], HITRAN08 [2], Rank et al. [18] and Hase et al. [21].

Line	Line positions (cm^{-1})					Position differences (cm^{-1})			
	PS[a]	Pollock et al. /NIST [16,17][b]	HITRAN08 [2][c]	Rank et al. [18][d]	Hase et al. [21][e]	PS-Pollock et al./NIST	PS-HITRAN08	PS-Rank et al.	PS-Hase et al.
P47	4006.195212(886)		4006.2003	4006.1908(23)	4006.200		−0.0051	+0.0044	−0.005
P45	4019.947982(666)		4019.9518	4019.9434(23)	4019.951		−0.0038	+0.0046	−0.003
P40	4053.215660(303)		4053.2174	4053.2156(23)	4006.217		−0.0017	+0.0001	−0.001
P35	4084.877823(121)		4084.8785	4084.8754(23)	4084.878		−0.0007	+0.0024	+0.000
P29	4120.728522(31)	4120.728658(330)	4120.7287		4120.728	−0.000136(332)	−0.0002		+0.001
P25	4143.315439(10)	4143.315466(119)	4143.3155		4143.315	−0.000027(119)	−0.0001		+0.000
P20	4170.055148(3)	4170.055146(19)	4170.0551		4170.055	+0.000002(19)	+0.0005		+0.000
P12	4209.343176(1)	4209.343184(8)	4209.3432		4209.343	−0.000008(8)	−0.0000		+0.000
P7	4231.684966(1)	4231.6849726(3)	4231.6850		4231.685	−0.000006(3)	−0.0000		−0.000
R0	4263.837202(1)	4263.837197(3)	4263.8372		4263.837	+0.000005(3)	+0.0000		+0.000
R12	4203.623331(1)	4203.623335(3)	4203.6233		4203.623	−0.000004(3)	+0.0000		+0.000
R20	4324.409885(2)	4324.409820(10)	4324.4098		4324.409	+0.000065(10)	+0.0001		+0.001
R25	4335.031116(8)	4335.030876(30)	4335.0309		4335.030	+0.000240(31)	+0.0002		+0.001
R30	4343.807215(34)	4343.806614(125)	4343.8066	4343.8088(23)	4343.806	+0.000601(130)	+0.0006	−0.0016	+0.001
R35	4350.720089(108)	4350.718859(407)	4350.7189	4350.7169(23)	4350.718	+0.001230(42)	+0.0012	+0.0032	+0.002
R40	4355.751669(278)		4355.7495	4355.7480(23)	4355.749		+0.0022	+0.0037	+0.003
R45	4358.883890(618)		4358.8803	4358.8843(23)	4358.880		+0.0036	−0.0004	+0.004
R50	4360.098660(1241)		4360.0931		4360.093		+0.0056		+0.006
Mean and std. dev.						+0.00018(40)	+0.0001(24)	+0.0021(24)	+0.001(2)

[a] Positions are calculated from rovibrational constants determined from laboratory absorption spectra; values listed to 6 decimal places.
[b] Absolute line positions obtained by heterodyne technique using color center laser absorption spectroscopy. Positions are reported to 6 decimal places.
[c] Positions in [2] are calculated using the Dunham coefficients determined from ATMOS − FTS Solar CO lines by Farrenq et al. [22]. Positions are given to 4 decimal places.
[d] Laboratory measurements using a heated absorption tube. High-J transitions in the J=30–48 range were observed in their experiment. An estimated uncertainty of $\pm 0.0023\ cm^{-1}$ was reported for each line [18]. Positions are given to 4 decimal places.
[e] From solar spectra recorded by the ACE-FTS instrument [21]. Positions are taken from HITRAN (see their Table 3, although no reference to any specific version of HITRAN is provided) and given to 3 decimal places.

study compare well; but showing small systematic deviations from about P30–R30. The lines are well enough separated that the first order mixing theory works well. The measured line intensities in [3] were limited to a smaller range in $|m|$ of ~25 compared to the much larger range obtained (calculated using the derived intensity and Herman–Wallis coefficients listed in Table 4) in the present work. To fit the diverse datasets available for this study a non-Voigt line shape with both speed dependence and line mixing became necessary. Comparison among all available intensities reported in the literature is beyond the scope of this work and hence not attempted, especially since all of the earlier studies use different line shape models than that used here. Such comparisons have already been made in several previous works, e.g.[1–4] and only comparisons to those studies [2–4] are provided in this paper.

Table 4 shows that no large correlations between the intensity parameters S_v and the Herman–Wallis coefficients a_1, a_2 and a_3 are seen; the largest anti-correlation coefficient of −0.80 is between a_1 and a_3. An anti-correlation of −0.70 exists between band intensity and a_2. There are a few large correlations among the rotational constants B, D and H, but none are large enough to cause problems with the fit.

Fig. 4 demonstrates the numerical precision in the line intensities obtained from the multispectrum fit expressed as a percentage of the retrieved intensity (ratio of calculated intensity uncertainty to retrieved intensity multiplied by 100) versus m. Since the individual intensities were not determined, but only the band strength and Herman–Wallis coefficients, the uncertainties must again be determined by using Eq. (4). In this case S_v is q_1, a_1 is q_2, a_2 is q_3, and a_3 is q_4. There is still some dependence upon the rovibrational constants in Eq. (2) since the position and band center are in the calculation of the line intensity, but these sources of uncertainty are orders of magnitude smaller than those due to the band intensity and Herman–Wallis parameters and may be ignored. Table 4 provides the required uncertainties and correlation coefficients and the derivatives in Eq. (4) can be found by partial differentiation of Eqs. (2) and (3).

The statistical uncertainty in intensity varies from less than 0.005% (for $|m| \leq 20$) to almost 0.05% as $|m|$ increases from 20 to 50. Such high precision in the line intensities was obtained through the use of constraints and the careful determination of the relative gas amounts from the spectra themselves. It is estimated that the absolute accuracy of the individual line intensities is approximately 0.5–1%, limited by the uncertainties in the volume mixing ratio determinations, the remaining fit residuals, uncertainty in pressure, path length and temperature determinations, the uncertainty due to the number of dimers that may be present in the cell and the presence of collision-induced absorption, if any.

The known quantum mechanical constraints imposed in the fitting resulted in smoothly varying intensities and their associated uncertainties. The results shown in Fig. 4 are useful for understanding the challenge in establishing

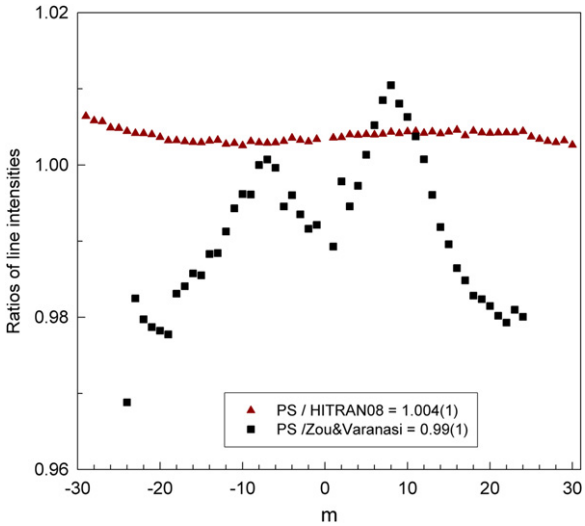

Fig. 3. Ratios of individual line intensities (for a natural CO abundance) retrieved from multispectrum fits to values in the HITRAN databases [1,2], and Zou and Varanasi [3] plotted as a function of m ($m=-J''$ for P branch and $J''+1$ for R-branch transitions). Line intensities determined by Brault et al. [4] have been adopted in the HITRAN [1,2] databases. Precisions plotted are smaller than the symbols used and are not visible. Brault et al. [4] used a value of 107.417 at 296 K as the rotational partition function. For comparison, the band strength reported in [4] has been scaled by a factor: (107.1134/107.417)=0.9972; and their band strength becomes $7.466(2)\times10^{-20}\times0.9972=7.445(2)\times10^{-20}$ cm/molecule at 296 K. Zou and Varanasi [3] reported a value of $7.532(66)\times10^{-20}$ cm/molecule at 296 K as their integrated band strength; but no value for the rotational partition function used was provided. Zou and Varanasi [3] used Voigt line shape, and these differences demonstrate the effect of using the wrong line shape.

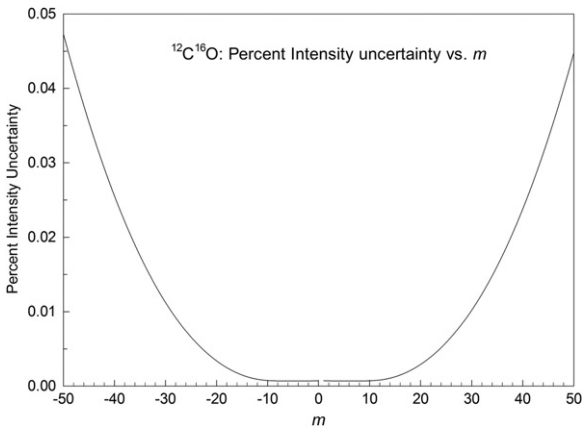

Fig. 4. The percent intensity uncertainties (ratio of intensity uncertainty to measured intensity multiplied by 100) are plotted as a function of m ($m=-J''$ for P branch and $J''+1$ for R-branch transitions). For the observed transitions in the range P30–R30, the uncertainties (excluding systematic errors) are still $\leq 0.012\%$. The uncertainties for the R-branch transitions are slightly smaller compared to the P-branch transitions. Although we do not know the exact reason for this, it might be due to the characteristics of spectral lines (e.g., closeness of lines, blend) in the two branches.

CO spectroscopic reference standards with the accuracies required to support atmospheric remote sensing. It must be emphasized that the absolute uncertainties (Table 2) are limited mainly by the signal-to-noise of the spectra and the contributions from other sources described above. The intensity uncertainties were smoothly J-dependent since line intensities were constrained to follow a theoretical relationship and the uncertainties follow the same formula (Eqs. (2) and (3)).

4.2. Self- and air-broadening coefficients

Similar to several previous studies (e.g., [12]), the self- and air-broadened Lorentz half width and self- and air-pressure-induced shift coefficients defined in Eqs. (5)–(7) were measured on a line-by-line basis in the constrained multispectrum fits:

$$b_L(p,T)=p\left[b_L^0(air)(p_0,T_0)(1-\chi)\left[\frac{T_0}{T}\right]^{n1}+b_L^0(self)(p_0,T_0)\chi\left[\frac{T_0}{T}\right]^{n2}\right] \tag{5}$$

$$v=v_0+p[\delta^0(air)(1-\chi)+\delta^0(self)\chi] \tag{6}$$

$$\delta^0(T)=\delta^0(T_0)+\delta'(T-T_0) \tag{7}$$

In Eqs. (5)–(7), b_L^0 and δ^0 represent pressure broadening and pressure-shift coefficients (in $cm^{-1}\,atm^{-1}$ at 296 K), respectively; b_L (p, T) is the Lorentz half width (in cm^{-1}) of the spectral line at pressure p and temperature T, b_L^0(Gas) (p_0, T_0) is the Lorentz half-width coefficient of the line at the reference pressure p_0 (1 atm) and temperature T_0 (296 K) of the broadening gas (either air or CO) and χ is the ratio of the partial pressure of CO to the total sample pressure in the cell. Temperature dependences of air- and self-broadened half-width and pressure-induced shift coefficients were measured separately for each transition within the same fit. As shown in Eq. (7) a linear model was used for the temperature dependence of pressure-induced shifts. Zou and Varanasi [3] used an exponential model to describe the variation of pressure-induced shifts with temperature analogous to the temperature dependence of pressure-broadened widths.

Broadening coefficients (self- and air-broadened widths) and the temperature dependence exponents for the broadening coefficients for unmeasured transitions were held fixed to values in the HITRAN08 compilation [2] and depend upon the rotational quantum number of the transition. Both the self- and air-induced shift coefficients for unmeasured lines were fixed to $-0.005\ cm^{-1}\,atm^{-1}$. In the analysis the temperature dependences for self- and air-shift coefficients were adjusted where appropriate. For unmeasured transitions their values were fixed to $+0.00002\ cm^{-1}\,atm^{-1}\,K^{-1}$. This assumption introduced no noticeable residuals in the least squares fits (see Fig. 1).

The measured widths and shifts, their temperature dependences and associated uncertainties and speed dependence parameters are listed in Tables 2 and 3 (positions, intensities and speed-dependent parameters are listed only in Table 2). The measured self- and air-broadened half-width coefficients as a function of m are plotted in Fig. 5. In panel (a) the measurements are compared to present air-broadened half-width coefficients and the self-broadened half-width coefficients of Brault et al. [4], Zou and Varanasi [3] and HITRAN08 [2]. In panels (b)–(d) the ratios of self-broadened half-width coefficients from present study with

results from Refs. [2–4] are plotted. The mean and the standard deviation in each case are given in the plots.

Based upon the recommendation of Brault et al. [4], spectral parameters (self-width and self-shift coefficients) were taken from their two sets of measurements (for transitions with $m \leq 23$ and $m > 23$) in generating the plots in 5(a) and 5(b). The discontinuity in the ratio seen in Fig. 5(b) (near $|m| = 24$) is due to this selection criterion. Fig. 5(a) shows the small but observable departure in the pattern of widths vs. m (near $m = 5$–12) of the Zou and Varanasi [3] from other plots. Zou and Varanasi [3] did not include line mixing and speed dependence in their analysis while the other studies considered both line mixing and speed dependence. Brault et al. [4] used dispersion (asymmetry) coefficients (first order line mixing or Rosenkranz line mixing) while the present study employed the full line mixing (off-diagonal relaxation matrix) in the analysis. Error bars are also included in these plots; but in the majority of cases they are not visible since their values are smaller than the size of the plot symbols used. The ratios of self-broadened half-width coefficients of present measurements with Zou and Varanasi [3] and HITRAN08 [2] are plotted in panels 5(c) and 5(d), respectively.

The measured air-broadened half-width coefficients vs. m are plotted in Fig. 6. Comparisons with HITRAN08 [2] and Zou and Varanasi [3] are included in Fig. 6(a). As reported by Smith et al. [24], the coefficients in HITRAN04 [1] and subsequently HITRAN08 [2] result from a fourth-degree polynomial fit to all air-broadening measurements of CO available in the literature at that time, assuming no vibrational dependence of the widths. Similar to self-broadened half-width coefficients vs. m in Fig. 5(a), small departure in the pattern of air-broadened half-width coefficients vs. m is

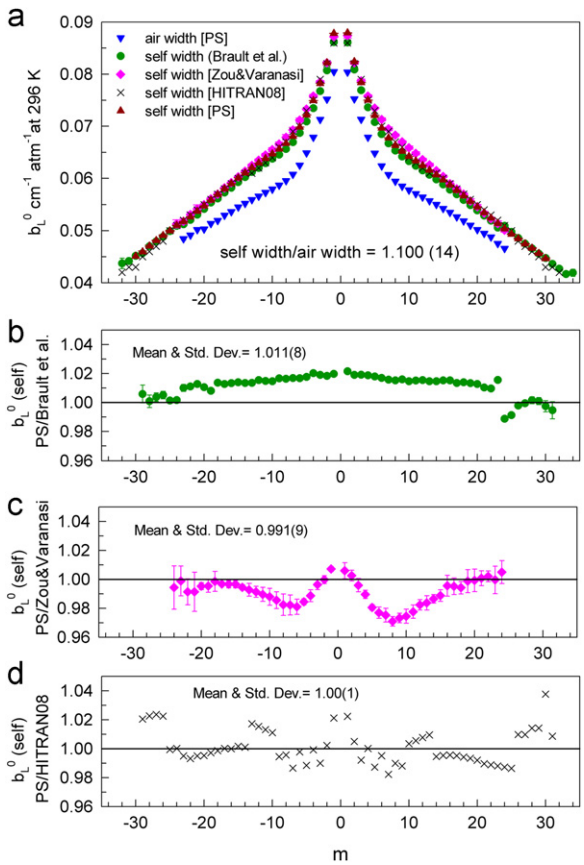

Fig. 5. (a) The measured self- and air-broadened half-width coefficients (cm^{-1} atm^{-1} at 296 K) from present study are plotted as a function of m ($m = -J''$ for P-branch transitions and $J''+1$ for R-branch transitions). The self-broadened half-width coefficients from Brault et al. [4], Zou and Varanasi [3] and HITRAN 08 [2] are shown for comparisons. Air-broadened half-width coefficients from present study are included for comparison between self- and air-broadening efficiencies in CO, (b) the ratios of self-broadened half- width coefficients between present study and Brault et al. [4], (c) the ratios of self-broadened half-width coefficients between present study and Zou and Varanasi [3], (d) the ratios of self-broadened half-width coefficients between present study and HITRAN databases [1,2]. Measured (one sigma standard deviation) uncertainties are shown where appropriate. Where no error bars are visible the uncertainties are smaller than the plot symbols used. The mean and standard deviations of the ratios are given in the respective panels. The width coefficients (self- and air-) in HITRAN databases [1,2] were provided by Smith et al. [24] using a 4th degree polynomial fit of laboratory measurements reported until 2004 (see the text for details). The ragged variations seen in panel (c) are due to the round off values for self-broadened half-width coefficients listed in HITRAN08 [2].

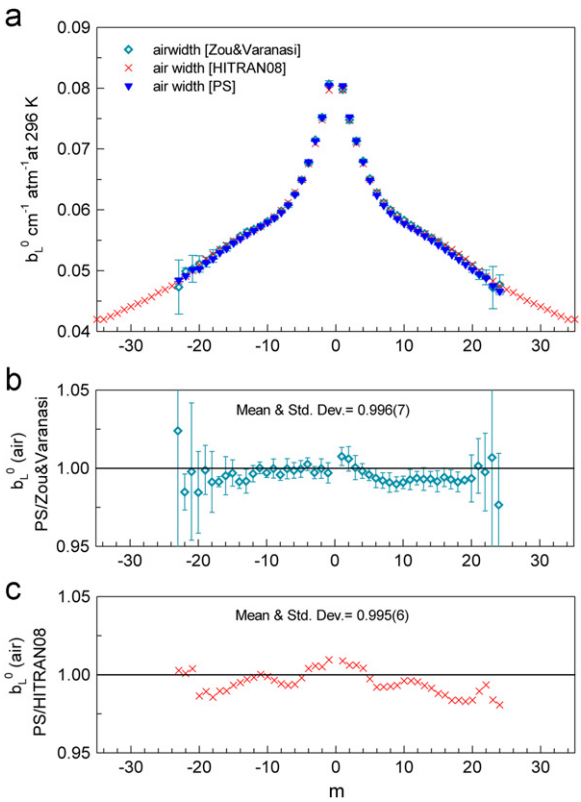

Fig. 6. (a) The measured air-broadened half-width coefficients (cm^{-1} atm^{-1} at 296 K) from this work are plotted as a function of m ($m = -J''$ for P-branch transitions and $J''+1$ for R-branch transitions). The air-broadened half-width coefficients from Zou and Varanasi [3] and from HITRAN databases [1,2] are included for comparison, (b) the ratios of air-broadened widths between present study and Zou and Varanasi [3], (c) the ratios of air-broadened widths between present study and HITRAN databases [1,2]. Measured (one sigma standard deviation) uncertainties are included where appropriate. Where no error bars are visible the uncertainties are smaller than the plot symbols used. The mean and standard deviations of the ratios are given in the respective panels.

evident near $m=5$–12 in the results between present study and Zou and Varanasi [3]. The ratios of air-broadened half-width coefficients obtained from the present study to those in Refs. [2,3] are plotted in Figs. 6(b) and (c), and the means and standard deviations of the ratios for individual spectral lines are also given when appropriate.

Both self- and air-broadening were measured simultaneously in the same multispectrum fit providing consistent parameters. Fig. 7 displays the ratios of self- to air-broadened width coefficients vs. m. Present results are shown in panel (a) and the corresponding ratios from Zou and Varanasi [3] and HITRAN08 [2] are plotted in panels (b) and (c), respectively. Similar to other molecular species (e.g. CO_2), the self-broadened widths of CO transitions are larger than the corresponding air-broadened widths; the ratios of self- to air-broadened width coefficients vary with m. These ratios are nearly 1.1 in all 3 cases. The curve in panel (c) does not show a smooth variation, similar to Fig. 5(c), and are due to the round off values used for self-broadened half-width coefficients listed in HITRAN08 [2]. The error bars representing the uncertainties are plotted in panels (a) and (b) but they are too small to be seen in Fig. 7a, except for a few high-J transitions.

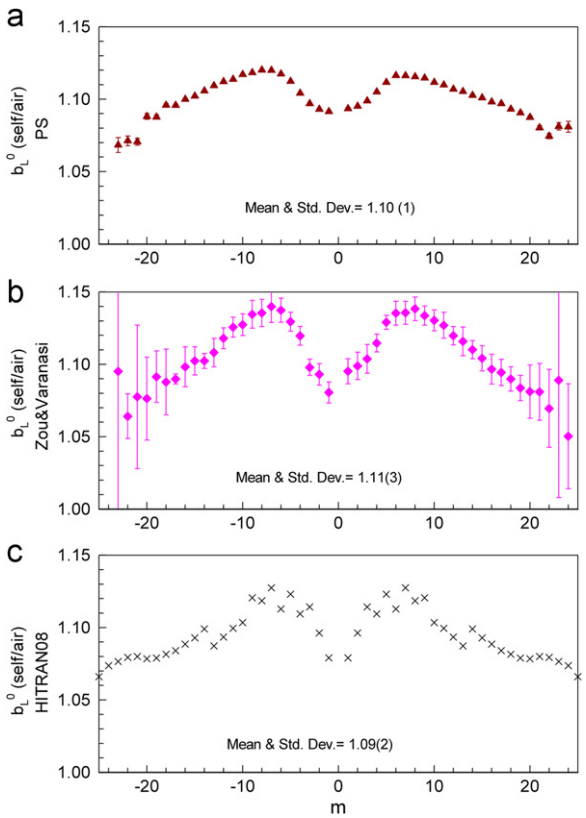

Fig. 7. The ratios of self- to air-broadened half-width coefficients vs. m ($m=-J''$ for P-branch transitions and $J''+1$ for R-branch transitions) are plotted, (a) present study, (b) Zou and Varanasi [3], (c) HITRAN databases [1,2]. These panels reveal the actual line-by-line variations in self- and air-broadened widths. Measured (one sigma standard deviation) uncertainties are included where appropriate. Where no error bars are visible the uncertainties are smaller than the plot symbols used. The mean and standard deviations of the ratios are given in the respective panels.

4.3. Self- and air- pressure-induced shift coefficients

The measured self-pressure-induced shifts coefficients as a function of m are shown in Fig. 8a. The error bars representing the uncertainties internal to the solution are plotted but they are too small (~0.1%) to be seen, except for a few high-J transitions. With the multispectrum technique it is essential that the wavenumber scales be precisely aligned from spectrum to spectrum. While pressure-induced shifts are a small effect, this precise wavenumber alignment combined with precise positions on the same scale produced by the constraints yields accurate pressure-induced shifts that are not affected by the absolute calibration of the wavenumber scales. The increased uncertainties observed at higher J are due to the weaker absorption strengths of these transitions. The uncertainties in [3] are much larger than those in the present study and in [4]. As noted in many previous studies the pressure-induced shifts are asymmetric between the P and the R branches. It is known that the pressure-induced shift coefficients are almost an order of

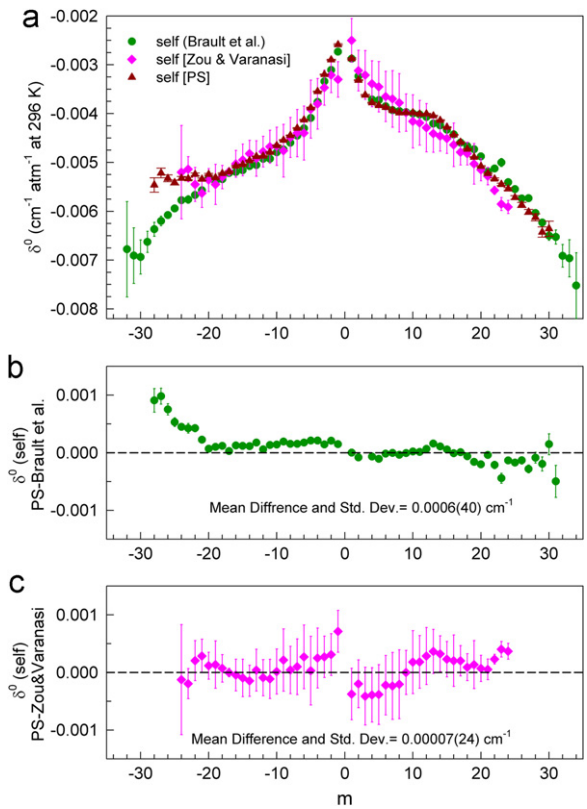

Fig. 8. (a) The measured self-pressure-induced shift coefficients (cm^{-1} atm^{-1} at 296 K) from this study are plotted as a function of m ($m=-J''$ for P-branch transitions and $J''+1$ for R-branch transitions). The self-shift coefficients from Brault et al. [4] and Zou and Varanasi [3] are included for comparisons. (b) The differences in self-shift coefficients between present study and Brault et al. [4], (c) differences in self-shift coefficients between present study and Zou and Varanasi [3]. Measured (one sigma standard deviation) uncertainties are included. Where no error bars are visible the uncertainties are smaller than the plot symbols used. The mean and standard deviations of the differences in the self-shift coefficients are given in the respective panels.

magnitude smaller than the pressure-broadened half-width coefficients. Even so fairly good agreement is seen among the 3 sets of values. The differences in the measured pressure-shift coefficients between the present measurements and Brault et al. [4] and between the present measurements and Zou and Varanasi [3] are displayed in panels (b) and (c). The mean pressure-induced shift coefficient differences for the individual lines with the standard deviations are given on the plots.

In Fig. 9a the measured air-pressure-induced shift coefficients vs. m in the $2\leftarrow 0$ band are shown. The only other high-resolution measurements of air-pressure-induced shift coefficients in the $2\leftarrow 0$ band are by Zou and Varanasi [3] and those values are also included in Fig. 9a. Except for a few low-m P-branch transitions the agreement is good. As explained in Ref. [24], the values in the HITRAN databases [1,2] for air-shift coefficients are from Zou and Varanasi [3]. The differences between the present measurements and [3] vs. m are shown in Fig. 9b. The mean and the standard deviation of the differences between the two sets are also given. The present set of values show much less uncertainty than the values in [3].

4.4. Temperature dependence of half-width and pressure-induced shift coefficients

The measured temperature dependence exponents for self- and air-broadened half-width coefficients are plotted as a function of m in Fig. 10. The results from the present study are shown in the upper panel (a) and those from

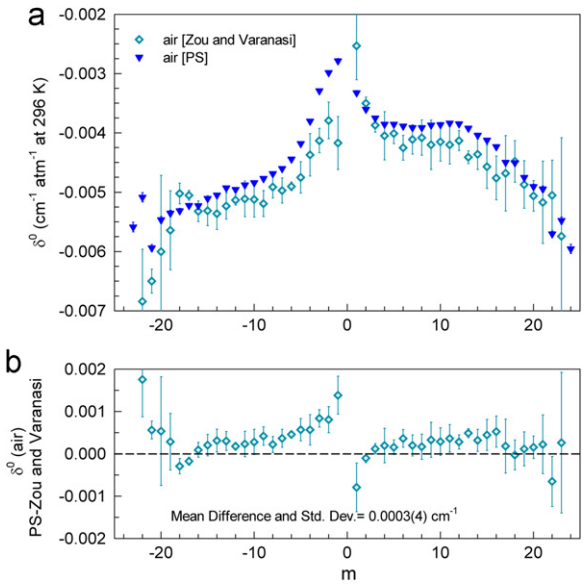

Fig. 9. (a) The measured air pressure-induced shift coefficients (cm^{-1} atm^{-1} at 296 K) from this study are plotted as a function of m ($m=-J''$ for P-branch transitions and $J''+1$ for R-branch transitions). The air-shift coefficients from Zou and Varanasi [3] are included for comparison. (b) The differences in air-shift coefficients between present study and Zou and Varanasi [3]. Measured (one sigma standard deviation) uncertainties are included. Where no error bars are visible the uncertainties are smaller than the plot symbols used. The mean and standard deviations of the differences in the air pressure-induced shift coefficients are given in panel (b).

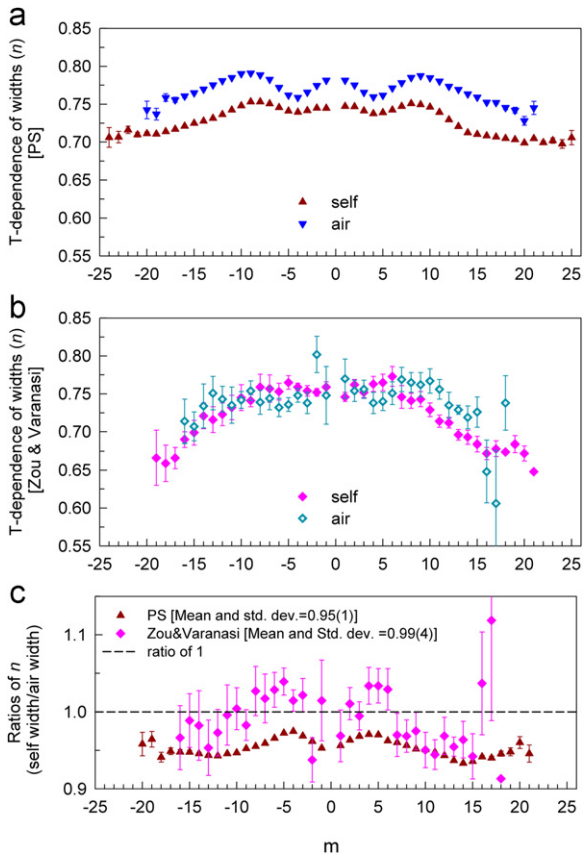

Fig. 10. Measured temperature dependence exponents ($\boldsymbol{n}$) of self- and air-broadened half-width coefficients are plotted vs. m ($m=-J''$ for P-branch transitions and $J''+1$ for R-branch transitions). (a) Present study and (b) Zou and Varanasi [3]. The ratios of $\boldsymbol{n}$ for self- and air-broadened width coefficients vs. m are plotted in (c). The mean and standard deviations of the ratios of $\boldsymbol{n}$ are given in panel (c). Measured (one sigma standard deviation) uncertainties are included. Where no error bars are visible the uncertainties are smaller than the plot symbols used.

Ref. [3] are plotted in (b). The temperature dependence exponents ($\boldsymbol{n}$) of the self-broadened half widths are smaller than those for air-broadened half widths. The values of $\boldsymbol{n}$ are m dependent, and the patterns observed for CO and air are similar. The same types of variations of $\boldsymbol{n}$ with m were observed by Zou and Varanasi [3] as displayed in Fig. 10b, although the exponents for self-broadened widths in [3] fall off more steeply to lower values at higher $|m|$. The two plots in Fig. 10c show the corresponding ratios of $\boldsymbol{n}$ for self- to air-broadening obtained in the present study and Ref. [3]. There are no other comprehensive experimental measurements for these parameters reported in the literature. The results in [3] do not show a smooth pattern in the R branch and have much larger uncertainties compared to the present values. The means of these ratios with standard deviations in the present study and Ref. [3] are 0.95(1) and 0.99(4), respectively. In both studies the minimum uncertainty in the half-width coefficients is in the middle of the temperature range measured. See the discussion below concerning pressure-induced shifts for the importance of this effect.

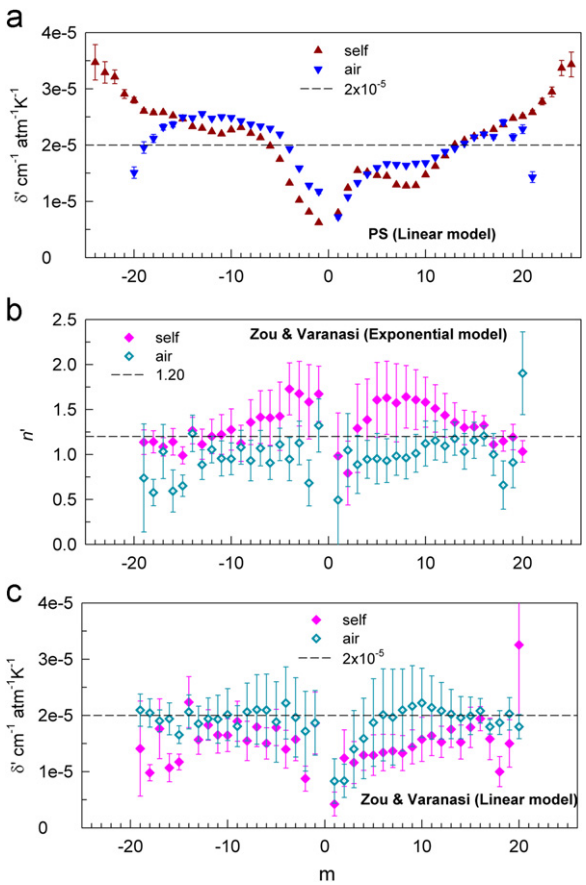

Fig. 11. (a) Measured temperature dependences of pressure-induced shift coefficients δ'(self) and δ' (air) from present study are plotted versus m ($m=-J''$ for P-branch transitions and $J''+1$ for R-branch transitions). All δ' values are positive, m-dependent and in general increase slowly from $\sim 0.5\times10^{-5}$ to 3.7×10^{-5} as $|m|$ increases for the measured transitions (except for a few P-branch lines in the case of air-induced shifts where it shows a small decrease for the weaker transitions ($m\geq 15$). (b) Measured temperature dependence exponents ($\boldsymbol{n}'$) for self- and air-induced shift coefficients by Zou and Varanasi [3] plotted versus m ($m=-J''$ for P-branch transitions and $J''+1$ for R-branch transitions). (c) The $\boldsymbol{n}'$ values converted to a linear model δ'at 296 K as given by Eq. (7) are shown in panel (c). Where error bars are not visible, the uncertainties are smaller than the plot symbols. See the text for details.

The measured temperature dependences for self- and air-induced shift coefficients δ' are plotted as a function of m in Fig. 11. The results from the present study are shown in Fig. 11a. The temperature dependences for both self- and air-induced shifts δ' are positive and vary from $\sim 0.5\times10^{-5}$ to $3.5\times10^{-5}\,\mathrm{cm^{-1}\,atm^{-1}\,K^{-1}}$ depending upon the quantum number m, generally increasing with m. An average value of $\delta'=2\times10^{-5}\,\mathrm{cm^{-1}\,atm^{-1}\,K^{-1}}$, shown by a dashed horizontal line, is recommended for unmeasured transitions. Because temperature dependences of pressure-induced shifts δ' are smaller than the already small values of pressure-induced shift coefficients δ^0 themselves, no further comparisons between the two sets (self- and air-) of δ' are meaningful. Except for a few cases ($|m|=15$–20) in the P branch for the temperature dependences of air- pressure-induced shift coefficients, both sets follow a similar pattern. Generally, δ' values for self-induced shifts are smaller than for air-induced shifts. The temperature dependence exponents for self- and air-induced shifts ($\boldsymbol{n}'$) from [3] are plotted in Fig. 11b. Zou and Varanasi [3] employed an exponential power law for the pressure-induced shift coefficients similar to the temperature dependence of width coefficients. Hence direct comparisons between the present measurements with those in [3] were not possible. Fig. 11b shows a clear separation between temperature dependences of the self- and air-induced shift coefficients. The horizontal dashed line in Fig. 11b corresponds to an arbitrarily chosen value of 1.2 separating the temperature dependence exponent $\boldsymbol{n}'$ representing self- and air-induced shift coefficients. The values of $\boldsymbol{n}'$ in Fig. 11b and reported in [3] were converted to the linear form at 296 K as given in Eq. (7) and plotted in Fig. 11c. This provides a more direct comparison with present results at 296 K. A horizontal dashed line corresponding to $\delta'=2\times10^{-5}\,\mathrm{cm^{-1}\,atm^{-1}\,K^{-1}}$ is arbitrarily drawn. In panel Fig. 11c it is clear that for Ref. [3] δ' for self-induced shifts are slightly smaller than the δ' for air-pressure-induced shift coefficients as is also evident in the values from present study shown in Fig. 11a. Similar to other line parameters, the uncertainties in [3] are larger than the present measurements.

The model used here to fit the temperature dependence exponent is quite simple but adequate for the temperature range available since there are no systematic residuals in the final fitted data to employ any other model or extra terms in the expression used.

Another means of comparing the pressure-induced shifts between the two studies is to compare the predicted pressure-induced shifts as a function of temperature within the model in which the study made measurements. Fig. 12a displays such a comparison for the air-induced shift coefficient of the P10 line. For the present study the width of the plotted line corresponds to the range of possible values within one standard deviation. This uncertainty level (shown by the width of the line) is computed as described in Eq. (8):

$$\varepsilon_\delta=\sqrt{\varepsilon^2_{\delta^0}+(T-T_0)^2\varepsilon^2_{\delta'}+2\rho_{\delta^0\delta}(T-T_0)\varepsilon_{\delta^0\delta'}} \tag{8}$$

The uncertainties, ε, in δ^0 and δ' are given in Table 3. For the P10 line the correlation, ρ, is 0.63318902 in our solution. This gives a functional form that allows the calculation of the uncertainty at any value of the temperature, T. As long as the functional form of the temperature dependence model is correct, the equation will provide an uncertainty that is correct for any temperature even if it is outside of the range of temperatures in the solution.

Also in Fig. 12a is a curve that represents the air-induced shift measured by Zou and Varanasi [3] with the power law model. While the present study covers spectra from 150 K to room temperature, the study by Zou and Varanasi [3] included only spectra in the range of 173.5 K to room temperature. These are the ranges plotted in the figure. The uncertainty as a function of temperature for Zou and Varanasi [3] cannot be determined from their study since the correlation coefficient in Eq. (8) was not given. One error bar is displayed at 296 K, the one temperature

for which they gave an uncertainty. This error bar, which is more than an order of magnitude larger than that of the present study, puts their room temperature value about one standard deviation from the present study. The two studies agree closely near the minimum uncertainty of the present study near 240 K (and likely near the minimum uncertainty of Zou and Varanasi [3]) and then separate slowly toward either sides of this temperature. It is likely that the two curves never separate by much more than one standard deviation of the values of Zou and Varanasi [3]. This indicates that where the pressure-induced shifts are best determined for this line, the two studies agree to within 1%.

Fig. 12b displays the uncertainty in the present air-shift coefficient for the P10 over the temperature range of the spectra. The minimum uncertainty is near the middle of the measured range of temperatures. This is contrary to the general expectation of a casual reader who sees only the pressure-induced shift at 296 K, its temperature dependence and their uncertainties. It is the correlation (last) term under the square root in Eq. (8) that provides the true information on the uncertainty of the pressure-induced shift with temperature. As in Fig. 12a, the uncertainty corresponding to $T=296$ K for the same line from [3] was much larger than in present study and falls far outside the vertical axis range shown in this figure. The measured uncertainty is minimum for a temperature of $T=245$ K.

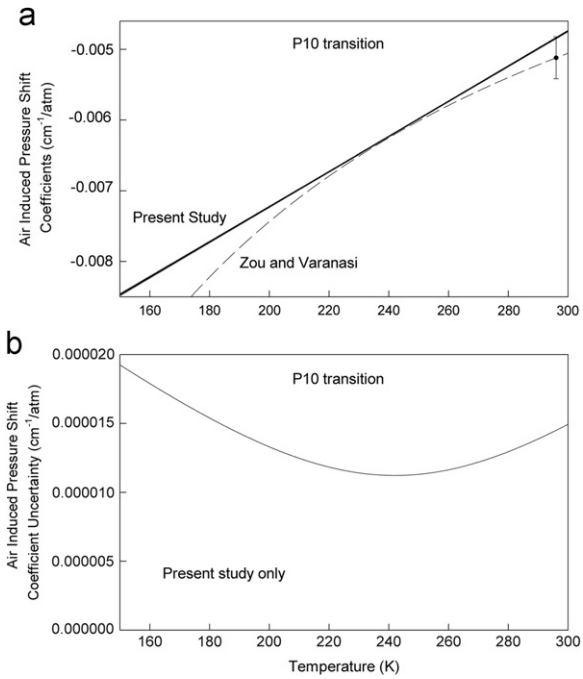

Fig. 12. (a) The variations in the measured air pressure-induced shift coefficient (δ^0 air) as a function of temperature (K) for a specific line P10 in the present study and in Ref. [3] are plotted. The uncertainties in the air pressure-shift coefficients as a function of temperature from the present study are represented by the variable thickness of the line drawn. In the case of Zou and Varanasi [3] only the uncertainty at 296 K is shown since no correlation coefficients were reported. The error bar in [3] is much larger than the uncertainties in the present study. Within one standard deviation, the pressure-induced shift coefficients overlap. In both cases the best measurement for δ^0 (air) is obtained near 245 K at the midpoint of the temperature range. For temperature dependence of pressure-induced shift coefficients, the present study used a linear model described by $\delta^0(T)=\delta^0(T_0)+\delta'(T-T_0)$while Zou and Varanasi [3] employed an exponential model given by $\delta^0(T)=\delta^0(T_0)(T_0/T)^{n'}$. (b) Uncertainties in the air-induced shift coefficients (δ^0air) for the example line P10 are plotted as a function of temperature (K). As in Fig. 12a, the uncertainty at $T=296$ K for the same line from [3] was much larger than in the present study and falls far outside the vertical axis range shown in this figure. The uncertainty obtained is minimum for $T=245$ K.

4.5. Line mixing and speed-dependent line shape

A conventional Voigt line shape was inadequate to fit all the data in the present study to within their noise levels. To minimize the statistical and systematic errors in the fit residuals, a non-Voigt line shape combining a speed-dependent line shape [25] with line mixing using the relaxation matrix formalism [23] was necessary. The relaxation matrix formalism was used in a similar manner to our previous studies (e.g., [12]). These off-diagonal relaxation matrix elements were determined only between pairs of neighboring lines. All other off-diagonal relaxation matrix element coefficients were set to zero. The retrieved self- and air-broadened off-diagonal relaxation matrix element coefficients (W_{ij}) in $cm^{-1}\,atm^{-1}$ at 296 K are listed in Table 6 and their temperature dependences in Table 7. In the absence of any low temperature spectra in previous studies (e.g., [12]), it was assumed that the temperature dependences of pressure-broadened widths, $\boldsymbol{n}$, also describe the temperature dependences of the off-diagonal relaxation matrix element coefficients. Because the present set included spectra recorded at both room- and cold temperatures it was possible to determine the temperature dependences of the off-diagonal relaxation matrix element~~s~~ coefficients (W_{ij}') for several transitions in the case of self-broadening. Since the optical densities of the spectra were not sufficiently high, and when the sample is cooled, the higher-J ($m\geq 15$) transitions become weaker quickly due to the Boltzmann distribution, the temperature dependence parameters were fixed to 0.7 for all air-broadened line mixing coefficients. The sum rule requires that the temperature dependence of the half-width and that of line mixing coefficients should on average be the same. Temperature dependence of the half-width coefficients is about 0.7 for most cases, and there were no prior experimental measurements on the temperature dependence of line mixing coefficients for any CO band until the present measurements. As shown in Table 6, the W_{ij} were fixed to default values of 0.01 or 0.005 $cm^{-1}\,atm^{-1}$ at 296 K for a few additional pairs of lines beyond the measured transitions (reasonable extrapolation from measured values) whose line mixing coefficients could not be reliably determined.

The measured off-diagonal relaxation matrix element coefficients for both self- and air-broadening are plotted as a function of m in Fig. 13a. The line mixing coefficients vary from $\sim$0.005 to $\sim$0.025 $cm^{-1}\,atm^{-1}$ at 296 K. Fig. 13a indicates that both self- and air- off-diagonal relaxation matrix element coefficients have comparable values. The values (both self- and air-) are not the same for transitions with same $|m|$ in the P and R branches, especially for air-broadening. Because a few self-broadened

Table 6
Self- and air-broadened off-diagonal relaxation matrix element coefficients[a] (W_{ij}) in the 2←0 band of $^{12}C^{16}O$.

Line mixing pair	Self-line mixing W_{ij}^{CO-CO}	Air line mixing W_{ij}^{CO-air}	Line mixing pair	Self-line mixing W_{ij}^{CO-CO}	Air line mixing W_{ij}^{CO-air}
P1 and P2	0.00570 (7)	0.00488 (14)	R0 and R1	0.00466 (4)	0.00674 (9)
P2 and P3	0.01080 (7)	0.01057 (15)	R1 and R2	0.01138 (5)	0.01528 (11)
P3 and P4	0.01472 (7)	0.01525 (15)	R2 and R3	0.01618 (6)	0.02039 (11)
P4 and P5	0.01734 (7)	0.01783 (16)	R3 and R4	0.01929 (5)	0.02325 (11)
P5 and P6	0.01908 (7)	0.01922 (17)	R4 and R5	0.02116 (5)	0.02462 (12)
P6 and P7	0.02019 (8)	0.01957 (20)	R5 and R6	0.02219 (5)	0.02527 (12)
P7 and P8	0.02086 (8)	0.01968 (22)	R6 and R7	0.02271 (5)	0.02542 (13)
P8 and P9	0.02124 (9)	0.01914 (26)	R7 and R8	0.02298 (6)	0.02513 (15)
P9 and P10	0.02132 (9)	0.01834 (30)	R8 and R9	0.02299 (6)	0.02445 (17)
P10 and P11	0.02110 (10)	0.01712 (36)	R9 and R10	0.02273 (6)	0.02310 (19)
P11 and P12	0.02005 (11)	0.01595 (44)	R10 and R11	0.02226 (6)	0.02135 (22)
P12 and P13	0.01829 (13)	0.01510 (53)	R11 and R12	0.02148 (6)	0.01922 (26)
P13 and P14	0.01704 (15)	0.01473 (63)	R12 and R13	0.02024 (7)	0.01728 (31)
P14 and P15	0.01558 (18)	0.01313 (75)	R13 and R14	0.01883 (8)	0.01544 (36)
P15 and P16	0.01336 (22)	0.01144 (86)	R14 and R15	0.01748 (10)	0.01293 (41)
P16 and P17	0.01242 (26)	0.00944 (93)	R15 and R16	0.01610 (12)	0.01121 (46)
P17 and P18	0.00972 (32)	0.01[b]	R16 and R17	0.01467 (14)	0.01035 (45)
P18 and P19	0.00784 (38)	0.01[b]	R17 and R18	0.01330 (17)	0.01[b]
P19 and P20	0.00393 (46)	0.01[b]	R18 and R19	0.01201 (21)	0.01[b]
P20 and P21	0.00434 (56)	0.005[b]	R19 and R20	0.01125 (25)	0.01[b]
P21 and P22	0.00344 (61)	0.005[b]	R20 and R21	0.01095 (31)	0.005[b]
P22 and P23	0.005[b]	0.005[b]	R21 and R22	0.01019 (38)	0.005[b]
P23 and P24	0.005[b]	0.005[b]	R22 and R23	0.00911 (45)	0.005[b]
P24 and P25	0.005[b]	0.005[b]	R23 and R24	0.00701 (53)	0.005 [b]
P25 and P26	0.005[b]		R24 and R25	0.00592 (55)	

[a] Units are cm^{-1} atm^{-1} at 296 K. The values given in parentheses represent one standard deviation measurement error in the last quoted digit.
[b] Fixed to default values of 0.01 cm^{-1} atm^{-1} or 0.005 cm^{-1} atm^{-1} as shown (reasonable extrapolation from the measured values in each branch).

spectra with higher path lengths (Table 1) were included in the solution line mixing parameters could be measured to a few higher-J values in the case of self-broadening than air-broadening. There are no other experimental measurements of off-diagonal relaxation matrix element coefficients to compare with the present data. In future measurements, use of longer absorption path lengths, higher optical densities and perhaps spectra at slightly elevated temperatures (not too high to excite too many molecules to higher vibrational levels) might provide better measurements of this rather important parameter in CO.

The Lorentz half width is not really a function of temperature, but a function of the speed of collisions between the molecules. The line shape at any given temperature is the weighted Lorentz profile over the various speeds of collision at that temperature. This weighting function is determined by the Boltzmann distribution, but the nature of the function describing the Lorentz width as a function of the speed of collision is not well known. For this study Eq. [9] was used [25]:

$$b_L^0(v) = b_L^0(v_m)\left(1 + S\left(\left(\frac{v}{v_p}\right)^2 - c\right)\right) \tag{9}$$

Here, v is the speed of the collision, v_m is the mean speed of collision, v_p is the most probable speed of collision such that $v_p = \sqrt{1.5}v_m$, c is taken to be 1.5 and S is the speed dependence parameter (SD) reported in this study.

The measured speed dependence for the 2←0 band of $^{12}C^{16}O$ listed in Table 2 and plotted in Fig. 13b indicates that reliable speed dependence was determinable only for transitions with $|m| \le 15$–18, and beyond those for ($20 < |m| < 30$), the absorptions were weak and the speed dependence showed much larger scatter in both branches. Fig. 13b shows that the speed dependence in the R branch is slightly larger than in the P branch for similar $|m|$. In the analysis it was assumed that the speed dependence is independent of the broadening gas and a single speed-dependent parameter was determined for both self- and air-broadening.

For a meaningful comparison of the Rosenkranz line mixing coefficients reported by Brault et al. [4] with present measurements, the off-diagonal relaxation matrix element coefficients from the present study reported at 296 K were converted to Rosenkranz line mixing coefficients in the low pressure limit (adequate for terrestrial atmospheric pressures) and plotted in Fig. 14. A reasonable agreement between the two sets of self-line mixing is seen for transitions with $|m| \le 15$ while large scatter is seen for transitions with $|m| > 15$. The numerical values of Rosenkranz line mixing from [4] converted from units of MPa to cm^{-1} atm^{-1} at 296 K are compared to present results at 296 K and listed in Table 8.

5. Conclusions

There are numerous experimental measurements of spectroscopic line parameters reported for CO in its fundamental, first and second overtone bands with spectra recorded at high resolution and high signal-to-noise. Some of those studies involve spectra recorded at various temperatures. Since it is not possible to list all the previous measurements or make comparisons with many of those results, in the present study comparisons are

Table 7
Temperature dependence exponents[a] (W_{ij}') of self-broadened off-diagonal relaxation matrix element coefficients, W_{ij}, for the 2←0 band of $^{12}C^{16}O$.

Mixing between	W_{ij}' for self-mixing	Mixing between	W_{ij}' for self-mixing
P1 and P2	1.027 (22)	R0 and R1	1.186 (15)
P2 and P3	1.033 (11)	R1 and R2	1.148 (8)
P3 and P4	1.068 (8)	R2 and R3	1.133 (6)
P4 and P5	1.116 (7)	R3 and R4	1.134 (5)
P5 and P6	1.119 (7)	R4 and R5	1.128 (4)
P6 and P7	1.097 (7)	R5 and R6	1.115 (4)
P7 and P8	1.041 (7)	R6 and R7	1.070 (4)
P8 and P9	0.963 (7)	R7 and R8	1.008 (4)
P9 and P10	0.839 (7)	R8 and R9	0.925 (4)
P10 and P11	0.727 (7)	R9 and R10	0.849 (4)
P11 and P12	0.7[b]	R10 and R11	0.771 (4)
P12 and P13	0.7[b]	R11 and R12	0.7[b]
P13 and P14	0.7[b]	R12 and R13	0.7[b]
P14 and P15	0.7[b]	R13 and R14	0.7[b]
P15 and P16	0.7[b]	R14 and R15	0.7[b]
P16 and P17	0.7[b]	R15 and R16	0.7[b]
P17 and P18	0.7[b]	R16 and R17	0.7[b]
P18 and P19	0.7[b]	R17 and R18	0.7[b]
P19 and P20	0.7[b]	R18 and R19	0.7[b]
P20 and P21	0.7[b]	R19 and R20	0.7[b]
P21 and P22	0.7[b]	R20 and R21	0.7[b]
P22 and P23	0.7[b]	R21 and R22	0.7[b]
P23 and P24	0.7[b]	R22 and R23	0.7[b]
P24 and P25	0.7[b]	R23 and R24	0.7[b]
P25 and P26	0.7[b]	R24 and R25	0.7[b]

[a] Temperature dependence exponents of line mixing coefficients (W_{ij}') are unitless. The values given in parentheses represent one standard deviation measurement error in the last quoted digit. Temperature dependence of off-diagonal relaxation matrix elements coefficients for air line mixing was not determinable and fixed to a default value of 0.7 for all transitions in both P and R branches and hence not reported in this table (see the text for details).

[b] Fixed to a default value of 0.7. The sum rule requires that on average the temperature dependence exponent of the half widths and that of the line mixing should average the same. Temperature dependence exponent of the half width is about 0.7 for most cases, and we did not have any values for CO line mixing until the present study was done.

made to only those measurements that are directly relevant. The results of Brault et al. [4] involved accurate self-broadened parameters from multispectrum fits of high-resolution high signal-to-noise spectra recorded at room temperature. Their measurements used non-Voigt line shapes including speed dependence and line mixing (using a different approach than the one used in this work). The only other high-resolution measurements of both self- and air-broadening in the 2←0 band as a function of temperature were by Zou and Varanasi [3] who used the conventional Voigt line shape without line mixing or speed dependence in the analyses.

The present study is unique because room and cold temperature spectra with both self- and air-broadening are fitted simultaneously over the entire band. Two low-pressure (~20 Torr) spectra of highly enriched (99% ^{13}C-enriched) ^{13}CO and (98% ^{18}O-enriched) $^{12}C^{18}O$ were included in the same least squares solution fitting the 2←0 bands of all three isotopologues. The analysis technique involved constraints for line positions and line intensities such that the rovibrational (G, B, D and H) and band intensity S_ν and Herman–Wallis coefficients (a_1, a_2, and a_3) were obtained

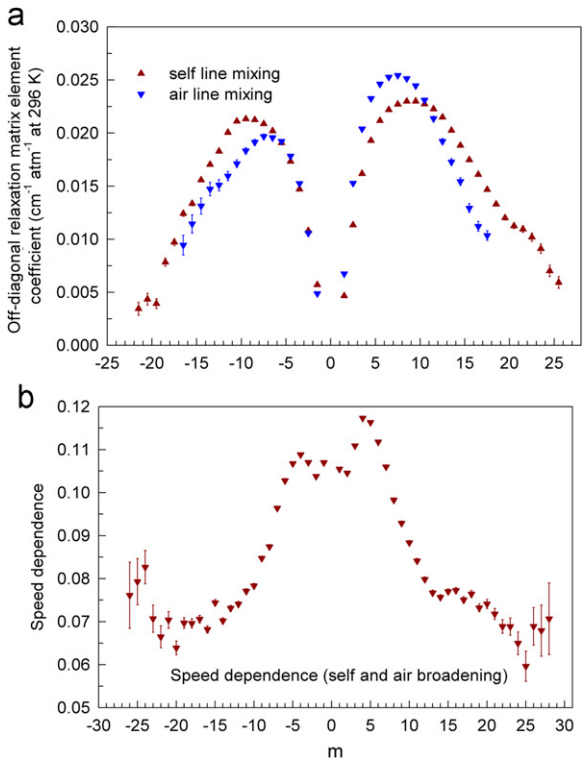

Fig. 13. Measured line mixing coefficients and speed-dependence parameters vs. m ($m=-J''$ for P-branch transitions and $J''+1$ for R-branch transitions) are plotted. (a) Measured off-diagonal relaxation matrix element coefficients (cm^{-1} atm^{-1} at 296 K) for self- and air-broadening. (b) Measured speed-dependence parameter in the P and R branches. The speed dependence is assumed to be independent of the broadening gases, and a single value common to both self- and air-line mixing is used to fit each transition. Where error bars are not visible, the uncertainties are smaller than the plot symbols used.

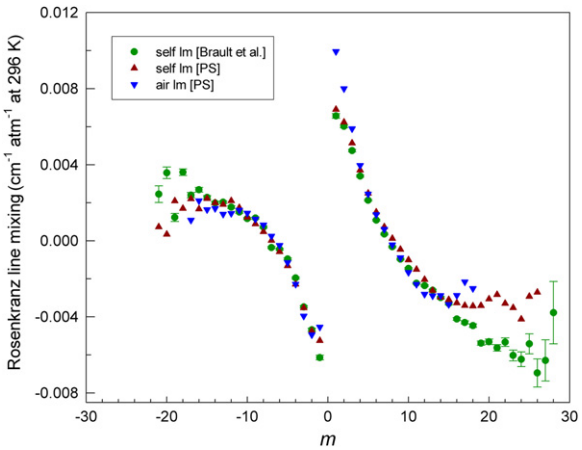

Fig. 14. The Rosenkranz line mixing coefficients are plotted as a function of m ($m=-J''$ for P-branch transitions and $J''+1$ for R-branch transitions). Results from Brault et al. [4] and present study (converted from off-diagonal relaxation matrix element coefficients) are compared. In the relaxation matrix formulation the Rosenkranz coefficients, positions, intensities and Lorentz widths are dependent upon temperature, but in this case those dependences are very small for pressures less than a few atmospheres.

Table 8
Rosenkranz line-mixing coefficients (cm^{-1} atm^{-1} at 296 K) for the 2←0 band of $^{12}C^{16}O$.

m	Self-line mixing		Self-line mixing	Air line mixing
	Brault et al.[a]	Unc.	Present study [b]	Present study [b]
−21	0.00245	0.00044	0.00073	
−20	0.00358	0.00030	0.00034	
−19	0.00123	0.00021	0.00210	
−18	0.00361	0.00017	0.00170	
−17	0.00240	0.00014	0.00220	0.00109
−16	0.00268	0.00012	0.00167	0.00210
−15	0.00228	0.00010	0.00222	0.00164
−14	0.00199	0.00008	0.00199	0.00170
−13	0.00203	0.00007	0.00191	0.00140
−12	0.00177	0.00007	0.00210	0.00144
−11	0.00151	0.00006	0.00174	0.00161
−10	0.00117	0.00005	0.00124	0.00145
−9	0.00120	0.00005	0.00089	0.00114
−8	0.00072	0.00005	0.00048	0.00083
−7	−0.00036	0.00005	0.00002	0.00024
−6	−0.00045	0.00005	−0.00057	−0.00024
−5	−0.00095	0.00005	−0.00132	−0.00114
−4	−0.00196	0.00005	−0.00228	−0.00229
−3	−0.00348	0.00006	−0.00353	−0.00395
−2	−0.00468	0.00008	−0.00474	−0.00494
−1	−0.00614	0.00012	−0.00525	−0.00453
1	0.00657	0.00012	0.00691	0.00990
2	0.00602	0.00007	0.00623	0.00800
3	0.00474	0.00006	0.00513	0.00589
4	0.00340	0.00005	0.00372	0.00396
5	0.00213	0.00004	0.00250	0.00246
6	0.00184	0.00004	0.00151	0.00138
7	0.00035	0.00004	0.00073	0.00060
8	−0.00031	0.00004	0.00013	−0.00021
9	−0.00096	0.00004	−0.00045	−0.00089
10	−0.00146	0.00004	−0.00101	−0.00166
11	−0.00224	0.00004	−0.00151	−0.00229
12	−0.00236	0.00004	−0.00204	−0.00281
13	−0.00260	0.00005	−0.00262	−0.00289
14	−0.00299	0.00005	−0.00297	−0.00288
15	−0.00330	0.00006	−0.00310	−0.00335
16	−0.00411	0.00007	−0.00327	−0.00287
17	−0.00430	0.00008	−0.00341	−0.00216
18	−0.00446	0.00009	−0.00343	−0.00251
19	−0.00538	0.00011	−0.00340	
20	−0.00531	0.00014	−0.00306	
21	−0.00563	0.00017	−0.00283	
22	−0.00533	0.00022	−0.00330	
23	−0.00603	0.00028	−0.00352	
24	−0.00623	0.00039	−0.00412	
25	−0.00542	0.00052	−0.00292	
26	−0.00695	0.00074	−0.00271	
27	−0.00629	0.00108		
28	−0.00378	0.00164		

[a] The first order line mixing (dispersion parameter, $1/\xi$) given in Brault et al. [4] is converted to units of cm^{-1} atm^{-1} at 296 K, using 1 MPa = 9.869232667 atm.

[b] The off-diagonal relaxation matrix elements coefficients measured in the present study are converted to first order line mixing (Rosenkranz parameters) coefficients using the conversion factors [23].

directly from the multispectrum fits. As a result, calculated line positions and intensities could be extrapolated to higher values of J than experimentally measured with uncertainties following the same systematic formula as the positions and intensities. Comparisons of few line shape parameters with recent measurements showed reasonably good agreement considering the entirely different analysis techniques used in those studies. The present study was undertaken to measure the first experimental self-broadening measurements with temperature exponents in the 2←0 band of CO. The present measurements are the only experimental study where line mixing parameters were retrieved applying the off-diagonal matrix element formalism. In a few instances for self-line mixing it was possible to measure the temperature dependence exponents for the off-diagonal relaxation matrix elements of several P- and R-branch transitions. Dicke narrowing was evident and required to fit the 20 Torr spectra when only a few low pressure spectra were included in the fit. These narrowing parameters were generally observed to be m-dependent. However, Dicke narrowing parameters could not be determined when higher pressure spectra were added to the multispectrum fits where this narrowing effect was probably masked by the speed dependence.

We have achieved the best precision as well as the best accuracy in all measured spectroscopic line parameters (except for line positions). The absolute accuracies in positions are ± 0.00005 cm^{-1} for transitions with $|m| \leq 20$ and ± 0.0001 cm^{-1} for those with $|m|$ in the 21–29 range. Rather than completely depending upon the thermistors and pressure gauge readings alone, small adjustments within the experimental uncertainties to the sample temperatures and volume mixing ratios of CO in air-broadened spectra (where appropriate) were necessary to minimize systematic errors in the final fits. Residual FTS phase errors and background polynomial fits were adjusted during the fitting processes. 100% transmittance levels and field of view corrections were applied where required and deemed necessary in reducing most of the systematic errors. Such corrections were small.

From simultaneous fit of several high resolution, high S/N spectra obtained at different experimental conditions of path length, pressure, temperature, self- and air-broadened spectra and using non-Voigt line shapes involving line mixing in the relaxation matrix formalism and speed dependence, a band strength value of $7.47326(5) \times 10^{-20}$ cm/molecule at 296 K for the 2←0 band of $^{12}C^{16}O$ was obtained. The value 107.1134 adopted in the HITRAN 08 database [2] was used for the rotational partition function. Brault et al. [4] by using a rotational partition function of 107.417 reported an integrated band strength value of $7.466(2) \times 10^{-20}$ cm/molecule at 296 K from their analysis. To compare the present result with the one reported in [4], a scaling factor of 0.9972 was applied to [4]. We then obtained a value of $7.445(2) \times 10^{-20}$ cm/molecule at 296 K. These results may be compared to $7.532(66) \times 10^{-20}$ cm/molecule at 296 K reported by Zou and Varanasi [3]. The value of Q_r used in [3] was not reported.

Some small residuals remain in the final fits as seen in Fig. 1d. Inclusion of speed dependence, line mixing and the van der Waals effect did not remove all the fit residuals. Some of these are probably related to unaccounted instrumental line shape characteristic of the Bruker FTS (such residuals do not appear in spectra recorded with the Kitt Peak FTS) especially when S/N is high and the absorption features are strong. The authors believe that theoretical development and interpretation on issues perhaps related to CO dimers and collision-induced absorption (CIA) might be required to account for the remaining fit residuals.

The spectral line parameters determined in this study are a complete set and owe their accuracy to the fact that they are derived in a manner consistent with each other. In order to attain the accuracy in simulations of the spectrum of the $2\leftarrow0$ band of $^{12}C^{16}O$, it is essential to use the entire set. An example of this is Fig. 12b. If the pressure-induced shift at 296 K is taken from source A and its temperature dependence is taken from source B, there is a correlation of zero between these two parameters. The uncertainty of the derived pressure-induced shift is the same at 296 K as that given by source A. However, the uncertainty is greater than that at every lower temperature due to loss of the last term under the square root in Eq. [8]. If source A reports an uncertainty for the temperature dependence close to that of source B and the correlation is greater than zero, the shift is less uncertain at every temperature below 296 K than if the uncorrelated value from source B is used. A similar situation holds for the highly correlated Lorentz half width and its temperature dependence, the position and the pressure-induced shift, the intensity and Lorentz half width and the line mixing and its temperature dependence. While not as obviously correlated, all of the parameters are related to some extent in the solution in this manner. Ideally, all correlations within the solution should be reported, but in the present case this would be a list with nearly 300,000 values! It is the nature of the multispectrum fitting technique and a single fit for the entire band that all of the correlations are handled in an optimum fashion.

Similar multispectrum analyses of $^{13}C^{16}O$ and $^{12}C^{18}O$ air-broadening as a function of temperature in the $2\leftarrow0$ band are in progress [26].

Acknowledgments

The authors dedicate this article honoring Drs. Jean-Marie Flaud, Claud Camy-Peyret and Alain Barbe for their invaluable contributions and impact on the theoretical and experimental aspects of the molecular spectroscopy and atmospheric remote sensing. V. Malathy Devi is especially thankful to Drs. Flaud and Camy-Peyret for the fruitful collaboration for many years on the analysis of the infrared spectra of O_3 and its isotopologues; and to Dr. Flaud for collaboration on the analysis of the infrared spectra of ethylene. The research performed at the College of William and Mary, Connecticut College and NASA Langley Research Center is supported by NASA's ASCENDS program. The research at the Jet Propulsion Laboratory (JPL) is performed under contract with National Aeronautics and Space Administration. A. Predoi-Cross is grateful for the support for this project provided by the Natural Sciences and Engineering Research Council of Canada. The authors thank M. Dulick of NOAO (National Optical Astronomy Observatory) for the assistance in obtaining some of the data used in this study.

References

[1] Rothman LS, Jacquemart D, Barbe A, Benner DC, Birk M, Brown LR, et al. The HITRAN 2004 molecular spectroscopic database. J Quant Spectrosc Radiat Transfer 2005;96:139–204.

[2] Rothman LS, Gordon IE, Barbe A, Benner DC, Bernath PF, Birk M, et al. The HITRAN 2008 molecular spectroscopic database. J Quant Spectrosc Radiat Transfer 2009;110:533–72.

[3] Zou Q, Varanasi P. New laboratory data on the spectral line parameters in the 1-0 and 2-0 bands of $^{12}C^{16}O$ relevant to atmospheric remote sensing. J Quant Spectrosc Radiat Transfer 2002;75:63–92.

[4] Brault JW, Brown LR, Chackerian Jr. C, Freedman R, Predoi-Cross A, Pine AS. Self-broadened $^{12}C^{16}O$ line shapes in the $v=2\leftarrow0$ band. J Mol Spectrosc 2003;222:220–39.

[5] Rosenkranz PW. Shape of 5 mm oxygen band in atmosphere. IEEE Trans Antennas Propag 1975;AP-23:498–506.

[6] Varanasi P. Measurements of line widths of CO of planetary interest at low temperatures. J Quant Spectrosc Radiat Transfer 1975;15:191–6.

[7] Nakazawa T, Tanaka M. Intensities, half-widths and shapes of spectral lines in the fundamental band of CO at low temperatures. J Quant Spectrosc Radiat Transfer 1982;28:471–80.

[8] Bouanich JP. Lineshifts in the first overtone band of CO self-perturbed and perturbed by N_2 at 298, 193 and 133 K. Can J Phys 1983;61:919–22.

[9] Bouanich JP. On the temperature dependence of self-broadening in the first overtone band of CO. J Quant Spectrosc Radiat Transfer 1984;31:564–7.

[10] Bouanich JP, Bermejo D, Domenech JL, Martinez RZ, Santos J. Pressure-induced lineshifts in the 2-0 band of CO self-perturbed and perturbed by He, Kr, O_2 and N_2. J Mol Spectrosc 1996;179:22–31.

[11] Benner DC, Rinsland CP, Devi VM, Smith MAH, Atkins D. A multispectrum nonlinear least squares technique. J Quant Spectrosc Radiat Transfer 1995;53:705–21.

[12] Devi VM, Benner DC, Brown LR, Miller CE, Toth RA. Line mixing and speed dependence in CO_2 at 6348 cm^{-1}: positions, intensities, and air- and self-broadening derived with constrained multispectrum analysis. J Mol Spectrosc 2007;242:90–117.

[13] Letchworth KL, Benner DC. Rapid and accurate calculation of the Voigt functions. J Quant Spectrosc Radiat Transfer 2007;107:173–92.

[14] Chackerian Jr C, Freedman R, Giver LP, Brown LR. Absolute rovibrational intensities and self-broadening and self-shift coefficients for the $X^1\Sigma^+ V=3\leftarrow V=0$ band of $^{12}C^{16}O$. J Mol Spectrosc 2001;210:119–26.

[15] Sung K, Mantz AW, Smith MAH, Brown LR, Crawford TJ, Devi VM, et al. Cryogenic absorption cells operating inside a Bruker IFS-125HR: First results for $^{13}CH_4$ at 7 μm. J Mol Spectrosc 2010;262:122–34.

[16] Maki A.G., Wells J.S. Wavenumber calibration tables for heterodyne measurements. Diane Publishing; 1991 [also available as NIST (National Institute of Standards and Technology) special publication 821 at 〈www.physics.nist.gov〉.

[17] Pollock CR, Peterson FR, Jennings DA, Wells JS, Maki AG. Absolute frequency measurements of the 2-0 band of CO at 2.3 μm; calibration standard frequencies from high resolution color center laser spectroscopy. J Mol Spectrosc 1983;99:357–68.

[18] Rank DH, ST. Pierre AG, Wiggins TA. Rotational and vibration constants of CO. J Mol Spectrosc 1965;18:418–27.

[19] Bijl LA, Kuiper GP, Cruikshank DP. Arizona-NASA atlas of the infrared solar spectrum. Report VIII. Communications of the Lunar and Planetary Laboratory 1969;9:93–120.

[20] Benner DC, Kuiper GP, Randić L, Thomson AB. Arizona-NASA atlas of the infrared solar spectrum. Report X. Communications of the Lunar and Planetary Laboratory 1972;9:155–69.

[21] Hase F, Wallace L, McLeod SD, Harrison JJ, Bernath PF. The ACE-FTS atlas of the infrared solar spectrum. J Quant Spectrosc Radiat Transfer 2010;111:521–8.

[22] Farrenq R, Guelachvili G, Sauval AJ, Grevesse N, Farmer CB. Improved Dunham coefficients for CO from the infrared solar lines of high rotational excitation. J Mol Spectrosc 1991;149:375–90.

[23] Levy A, Lacome N, Chackerian Jr C. Spectroscopy of the Earth's atmosphere and interstellar medium. In: Rao KN, Weber A, editors. Collisional line mixing. Boston: Academic Press; 1992. p. 261–337.

[24] Smith M.A.H., Brown L.R., Devi V.M., Pittman T.J. CO broadening and shift parameters for TES. In: Proceedings of the eighth HITRAN database conference, Cambridge, MA, June 15–18, 2004.

[25] A. Vitcu, Line shape studies in the 0310-0110 Q branch of N_2O using a mid-infrared difference-frequency spectrometer. Dissertation, University of Toronto 2003.

[26] V. Malathy Devi, D. Chris Benner, M.A.H. Smith, A.W. Mantz, K. Sung, L.R. Brown, Spectral line parameters including temperature dependences of air-broadening for the $2\leftarrow0$ bands of $^{13}C^{16}O$ and $^{12}C^{18}O$ at 2.3 μm, in preparation.